

CERTIFICATION OF APPROVAL

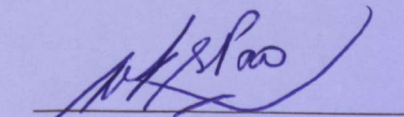
GEOMECHANICS RELIABILITY MODELING FOR DE-RISKING

By

Cheng Lee Chon

A project dissertation submitted to the
Mechanical Engineering Programme
Universiti Teknologi PETRONAS
in partial fulfilment of the requirement for the
BACHELOR OF ENGINEERING (Hons)
(MECHANICAL ENGINEERING)

Approved by,

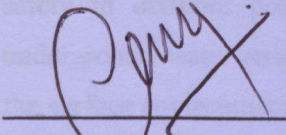


(Dr William Pao)

UNIVERSITI TEKNOLOGI PETRONAS
TRONOH, PERAK
MAY 2012

CERTIFICATION OF ORIGINALITY

This is to certify that I am responsible for the work submitted in this project, that the original work is my own except as specified in the references and acknowledgements, and that the original work contained herein have not been undertaken or done by unspecified sources or persons.



(CHENG LEE CHON)

ABSTRACT

One of the most common geomechanics problems is reservoir compaction and its associated land surface subsidence. This problem is complex and the affected geomechanics parameters vary across the underground formation. Subsidence causes major environmental concerns, leading to risk of flooding in land operations or platform safety in offshore production. The same problem in hydrocarbon production and underground water removal has significant impact to both the exploitation scheme and the surface environments. Previous researches focused on examining the displacement of the subsided area and its stress field by assuming the geomechanics properties of the reservoir and its surrounding to be homogeneous. However, geomechanical medium is typically complex and inhomogeneous. Some other researches assume variation of one parameter to be independent of the rest of other parameters. This confines the investigation by looking at specific geomechanics parameters in certain region only. Consequently, the parameters cannot be de-risked in a holistic manner with these assumptions. This project intends to propose a geomechanical de-risking workflow that utilizes components such experimental design, tornado chart, Multi-Variate Regression (MVR), and First Order Reliability Method (FORM). The Geomechanics tool will be treated as 'black box' engine that generate desired responses.

ACKNOWLEDGEMENT

First of all, the author would like to thank the Almighty God for providing him with blessings, strength and health to work on the final year project. The whole experience would not be made possible without the guidance and protection from the Lord. Also, the author would like to thank his family members for all the support and encouragement throughout the one year experience.

The author is also grateful for the continuous supervision and support of his supervisor, Dr. William Pao from the Mechanical Engineering Department of UTP. This Report would not have been possible without the kind support and assistance from him.

Last but not least, the author would like to thank the SEDEX 30 organizing committee as well as URPC organizing committee for their hard work and support in providing a platform to showcase the author's project.

1.1 Introduction of subsidence behavior	1
1.2 History occurrence of subsidence	2
1.3 Nucleus of Strain	2
1.3.1 Assumption of Geotens Nucleus of Strain	2
1.4 Uncertainty in Geomechanics	8
1.5 Safety Factor and Probabilistic Geomechanics Method	9
1.5.1 Design of Experiment (DOE) and Response Surface Method (RSM)	10
1.5.2 Surface Response Model	12
1.5.3 Risk Matrix and reliability index	13
Chapter 3: Methodology	13
3.1 Flow of Methodology	13
3.1.1 Geomechanics Model Building	13
3.1.2 Probabilistic Geomechanics Workflow	13
Step A - Geomechanics Requirement	13
Step B - Experimental Design	14
Step C - Geomechanics Engine	14

Table of Contents

Step 4 - Multiple Regression	14
Step 5 - Reliability Assessment	15
Step 6 - Interpretation Tools	18
Table of Contents	
Certification of Approval	i
Certification of Originality	ii
Abstract	iii
Acknowledgement	iv
List of Figures	vii
List of Tables	vii
Chapter 1: Introduction	1
1.1 Opening Remarks and Background Study	1
1.2 Causes and Consequences of Subsidence	2
1.4 Problem Statements	4
1.5 Objectives and Scope of Study	4
Chapter 2: Literature review	5
2.1 Introduction of subsidence behavior	5
2.2 History occurrence of subsidence	6
2.3 Nucleus of Strain	7
2.3.1 Assumption of Geertsma Nucleus of Strain	8
2.4 Uncertainty in Geomechanics	8
2.5 Safety Factor and Probabilistic Geomechanics Methods	9
2.5.1 Design of Experiment (DOE) and Response Surface Method (RSM)	10
2.5.2 Surface Response Model	12
2.5.3 Risk Matrix and reliability index	12
Chapter 3: Methodology	13
3.1 Flow of Methodology	13
3.1.1 Geomechanics Model Building	13
3.1.2 Probabilistic Geomechanics Workflow	13
Step A - Geomechanics Requirement	13
Step B – Experimental Design	14
Step C – Geomechanics Engine	14

Step D - Multi-Variate Regression.....	14
Step E - Reliability Assessment.....	15
3.2 Prototyping the Integrated Tools.....	18
3.3 Equipment Used.....	18
3.4 Gantt Chart.....	19
Chapter 4: Results and Discussion.....	21
4.1 Probabilistic Geomechanics Workflow.....	21
4.1.1 Geomechanics model.....	21
4.1.2 Validation and Discussion on Geomechanics Model.....	23
4.2 DoE, Geomechanics Engine and MVR.....	29
Chapter 5: Prototype.....	34
5.1 Probabilistic De-Risking Workflow, “ProWork”.....	34
5.2 Geomechanical Base Model.....	35
5.3 Probabilistic Geomechanics Model.....	37
5.4 Help function for users.....	40
Chapter 6: Conclusion.....	41
REFERENCES.....	42
APPENDIX.....	45

Figure 3.3 Geostatic Descriptions for base model.....	36
Figure 3.4 Compressibility Effect due to Pressure Depletion on Graphical User interface.....	36
Figure 3.5 Suggested Safety Factor.....	37
Figure 3.6 User Interface of De-Risking Workflow.....	38
Figure 3.7 Graphical details on ProWork.....	39
Figure 3.8 Probability Table Generation.....	39
Figure 3.9 Help Page on ProWork.....	40

List of Tables	
TABLE 1 Reservoir Properties for Anderson Sea field (1996 to 2008).....	21
TABLE 2 Upper and lower range of uncertainties for reservoir model.....	23
TABLE 3 Air cap design level for M1, M2, T4, T20 platform.....	25
TABLE 4 Rock mechanic properties of P20.....	26
TABLE 5 Rock Mechanic properties of P4.....	27
TABLE 6 Depletion pressure for M1's, M2, T4 and T20 platform from 1996 to 2008.....	28
TABLE 7 Subsidence observed at M1, M2, T4 and T20 platform from 1996 to 2008.....	28

List of Figures

Figure 1.1 Possible effects of petroleum production	2
Figure 1.2 Figure 1.2 Subsidence at San Joaquin Valley southwest of Mendota, California.....	2
Figure 1.3 Subsidence caused by mining, trough subsidence.....	3
Figure 2.1 Overview of occurrence of land subsidence.....	5
Figure 2.2 Illustration of compaction at reservoir and land subsidence	5
Figure 2.3 Places and time subsidence occurs in history	6
Figure 2.4 Geometry for Geertsma Solution by Geertsma (1973).....	7
Figure 2.5 Example of DOE used in Gas Field Development by Itotoi et al. (2010).....	11
Figure 3.1 Proposed Geomechanics workflow	16
Figure 3.2 Methodology Flow	17
Figure 4.1 Geomechanical model for probabilistic analysis.....	22
Figure 4.2 Comparison of VBA calculation and Analytical Solution from FJaer (2008).....	24
Figure 4.3 Percentage deviation between VBA solutions and Analytical solutions.....	24
Figure 4.4 Comparison between subsidences derived from GPS and VBA calculation	27
Figure 4.5 Excel output of Plackett-Burman design	29
Figure 4.6 Excel based Geertsma geomechanical engine	30
Figure 4.7 Tornado chart characterizing sensitivities of each parameters	31
Figure 4.8 Relative influence chart characterizing the relative impact of each parameters	31
Figure 4.9 True solution against the predicted solution with upper/lower bounds.....	32
Figure 4.10 True solution against the predicted solution using Monte Carlo simulation. Upper/lower bounds established from experimental design simulation	32
Figure 5.1 Excel Worksheet with Work Flow integrated	34
Figure 5.2 First Page of Work Flow.....	34
Figure 5.3 Geertsma Descriptions for base model	35
Figure 5.4 Compressibility Effect due to Pressure Depletion on Graphical User Interface	36
Figure 5.5 Suggested Safety Factor	37
Figure 5.6 User Interface of De-Risking Workflow	38
Figure 5.7 Graphs details on UserForm	39
Figure 5.8 Reliability Table Generation.....	39
Figure 5.9 Help Page on ProWork	40

List of Tables

TABLE 1 Reservoir Properties for Analytical Solution from Fjaer (2008).....	21
TABLE 2 Upper and lower range of uncertainties for reservoir model	23
TABLE 3 Air gap design limit of M1, M3, F6, F23 platform	25
TABLE 4 Rock mechanic properties of F23.....	26
TABLE 5 Rock Mechanic properties of F6	27
TABLE 6 Depletion pressure (in MPa) at M1, M3, F6 and F23 platform from 1996 to 2008.....	28
TABLE 7 Subsidence detected at M1, M3, F6 and F23 platform from 1996 to 2008	28

Chapter 1: Introduction

1.1 Opening Remarks and Background Study

One of the most common geomechanics problems described by Fjaer et al. (2008) and Zoback (2007) is reservoir compaction and its associated land surface subsidence. This problem has been recorded since subsidence was first observed in Goose Creek Oil Fields dated back in 1910s, Texas (Geertsma, 1973; Fjaer et al., 2008). Later, significant surface subsidence is also found in Wilmington field in California (Geertsma, 1973; Fjaer, 2008), Bolivar Coast in Venezuela (Mayuga et al., 1963; Baghdikian et al., 2010), Groningen Gas field in Netherlands (Schoonbeek et al., 1976; Mobach et al., 1994), and Ekofisk in Norway (Rentsch and Mes, 1988). In the United States alone, surface subsidence has been reported in at least 37 out of 50 states affecting an area of more than 80,000km² (Johnson, 1998).

Extensive researches (Geertsma, 1973; Zoback, 2008; Fjaer, 2008) have been carried out to describe the relationship between reservoir compaction and surface subsidence. One of the key assumptions in these researches is to consider the reservoir and its surroundings to be homogeneous. However, formation is an in-homogenous medium. The related properties used to describe subsidence vary across the layers of underground formation. Here, we are dealing with complex geology which has the behavior of a composite. We are also dealing with very limited site investigation data due to economic constraint (Fjaer, 2008) In order to overcome the limitation, probabilistic approach is widely used.

If we were to plot a histogram based on the multitude of data for one of the properties from the hypothetical site investigation, we would likely obtain a range of values in the form of a bell-shaped curve. The variability shown in these properties suggests that they can be highly amenable to a statistical interpretation (Fenton and Griffiths, 2008). We can then estimate the reliability of the formation by inputting the properties' means and variances. It is then useful to assess the risk associated with the formation and de-risking can be done based on the risk assessment.

1.2 Causes and Consequences of Subsidence

There are four main causes of subsidence, i.e. hydrocarbon production, mining, earthquake and groundwater/fluid removal (Knaap et al., 1967; Josept et al., 1972; Geertsma, 1973; Danielsen et al., 1988; Derek et al., 1989; Atashbari et al., 2007). The first one - also the most common one in oil and gas industry – is hydrocarbon production (Geertsma, 1973). Figure 1.1 shows an example of hydrocarbon production.

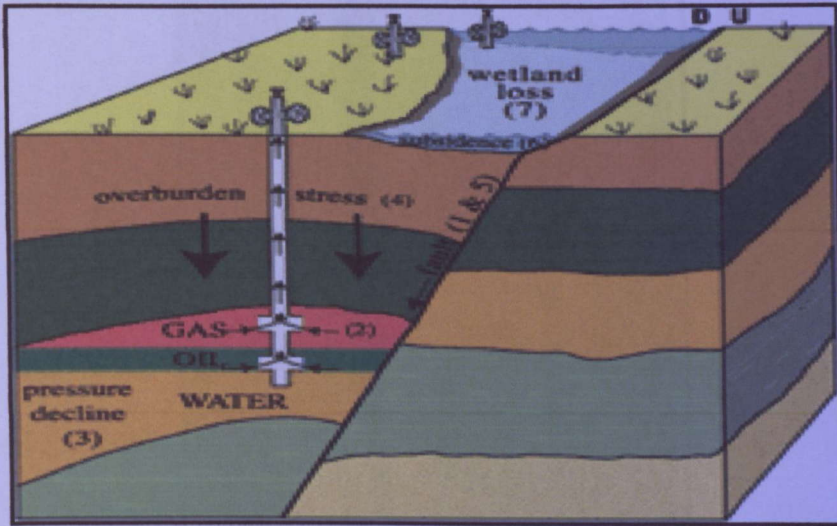


Figure 1.1 Possible effects of petroleum production
(Image from St. Petersburg Coastal and Marine Science Center)

Prolonged or rapid production of oil, gas, and formation water causes subsurface formation pressures to decline. The lowered pressures increase the effective stress of the overburden, which causes compaction of the reservoir rocks and may cause formerly active faults to be reactivated. The downward displacement along the faults causes land-surface subsidence.

One of the examples of subsidence due to oil and gas extraction was found at Mississippi River Delta. The average historical subsidence rate in the Mississippi delta is 12 mm/year (Shinkle and Dokka 2004). Furthermore, the subsidence at Mississippi River Delta due to oil and gas extraction has caused the ocean to rise and flood over 88 km² of land each year.

Subsidence caused by oil and gas extraction can reach as much as 9 meters over a short range of geological years. Figure 1.2 is an image taken in 1977 that shows a measurement of the subsidence occurred at one particular place.

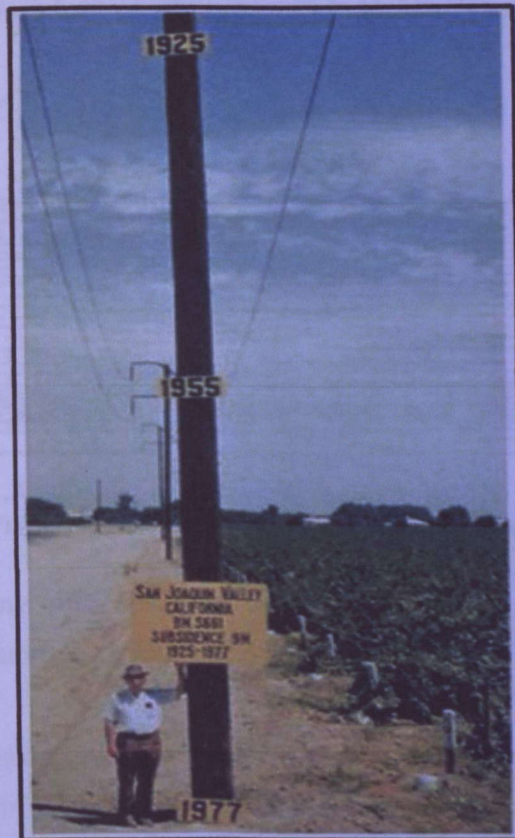
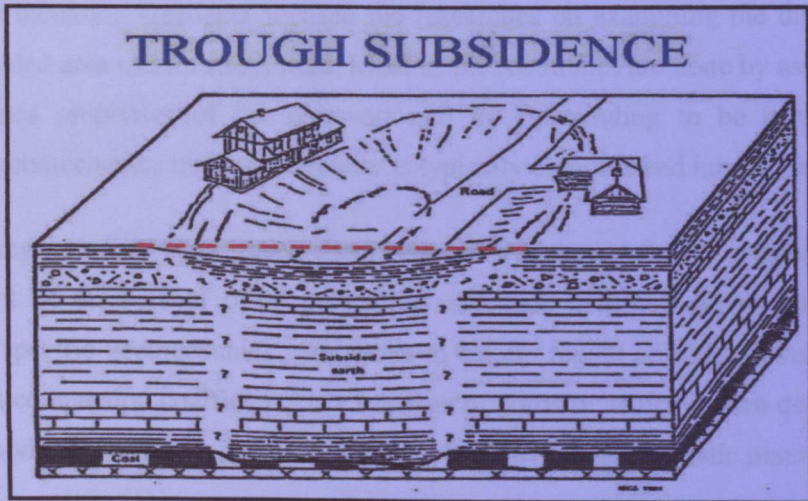


Figure 1.2 Subsidence at San Joaquin Valley southwest of Mendota, California. (Image from United States Geological Survey (USGS))

The picture was taken at a location of an approximate location of maximum subsidence in the United States identified by research efforts of Dr. Joseph F. Poland (pictured). The subsidence was estimated to be 9 meters over a period of 50 years.

Secondly, mining (Derek et al, 1989) is also another important factor that contributes to subsidence. Subsidence troughs induced by mining can be found at active or abandoned mines. It is difficult, if not impossible, to predict if or when failure in an abandoned mine might occur, since abandoned mines has the potential to collapse long after the

mining is completed, if the mine workings were not designed to provide long-term support. Figure 1.2 shows an example of subsidence caused by mining.



**Figure 1.3 Subsidence caused by mining, trough subsidence
(Image from Pennsylvania Departmental of Environmental Protection)**

The impact of mining subsidence on the environment can be very catastrophic, destroying property and even leading to the loss of life (Bell et al., 2000).

Another cause of subsidence is the excessive ground-water pumping (Atashbari et al., 2007) accompanied by the compaction of the unconsolidated aquifer system. The overdraft of such aquifer resulted ground failures and permanent subsidence. The corresponding subsidence leads to complete or partial loss of water due to leakage to the underlying strata (Bhattacharya and Singh, 1985).

Summing up all the factors that cause subsidence, it is realized that subsidence not only occurs around places nearby to hydrocarbon production but also any places with underground activities. As opposed to common belief, some of the subsidence occurs in places miles away from places of underground activities. Thus, a de-risking workflow is relevant and important to be proposed in this project. Many de-risking tools, like experimental design, reliability method, and risk assessment are already used in previous literatures. This project will further enhance the de-risking workflow and integrate the scattered but relevant de-risking workflows that are being used in the field.

1.4 Problem Statements

The most common problem in geomechanics is subsidence as discussed above. A few researchers including Geertsma focused the researches on examining the displacement of the subsided area and its stress field. Most of the researches are done by assuming the geomechanics properties of the reservoir and its surrounding to be homogeneous. However, geomechanics medium in reality is typically complex and inhomogeneous.

In de-risking practice also, researchers assume variation of one parameter to be independent of the rest of other parameters. So, this confines the investigation by looking at specific geomechanics parameters in certain region only. However, it is well known that compaction coefficients is a function of porosity; which in turn dependent on Young's modulus. Thus, the parameters cannot be de-risked in a holistic manner.

1.5 Objectives and Scope of Study

- 1) Propose a Geomechanics de-risking workflow. Components used include Experimental design, tornado chart, Multi-Variate Regression and reliability method.
- 2) Prototype a software for in-house usage of de-risking workflow complemented with Graphical User Interface (GUI).

The scope of study includes:

- 1) Overview of different probabilistic method.
- 2) The Geomechanics tool will be treated as 'black box' engine that generate desired responses.

Chapter 2: Literature review

In most cases, there is no simple rule or theory that describes the de-risking practice in geomechanics. This chapter will first describe the natural occurrence of subsidence. The theory used to calculate the subsidence. Then, an overview of safety factor used for risk analysis in geomechanics is outlined.

2.1 Introduction of subsidence behavior

One of the most common phenomenon described by Raaen et al. (2008) and Zoback (2007) of rock mechanical effects on reservoir scale behavior are reservoir compaction and associated surface subsidence. Figure 2.1 is a brief overview of how land subsidence occurs starting from underground hydrocarbon/water removal.



Figure 2.1 Overview of occurrence of land subsidence

Mask removal due to hydrocarbon/water activities causes depletion of pore pressure. Reduction of pore pressure from a reservoir will increase the effective stress and causes the rock itself to shrink. Reservoir will compact and in turn causes subsidence.

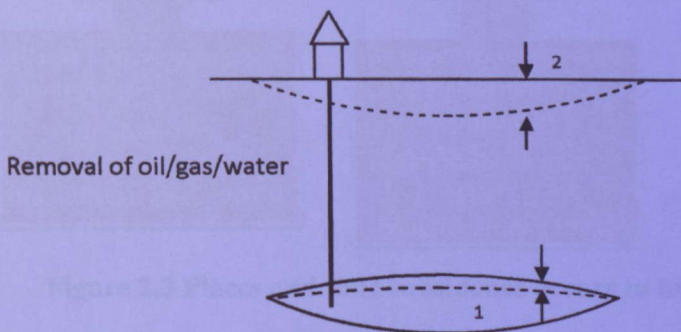


Figure 2.2 Illustration of compaction at reservoir (region 1) and land subsidence (region 2)

Subsidence occurs not only due to hydrocarbon production, it also happens due to the removal of underground water (Atashbari et al., 2007). Besides the specific problems introduced in chapter 1, subsidence also causes environmental concerns, leading to risk of flooding in land operations or platform safety concerns in offshore production. The same problem in hydrocarbon production studied by Wing (2004) and underground water removal (Waller and Roger, 1982) has significant impact to both the exploitation scheme and the surface environments. However, land subsidence is not so noticeable because it happens over an extensive area.

2.2 History occurrence of subsidence

Since subsidence was first recorded back in 1910s on Goose Creek, Texas, many other researchers have discussed on the topic of subsidence in literature. The important subsidence occurred in history is tabulated in the Figure 2.3 according to the time and place the subsidence was first recorded.

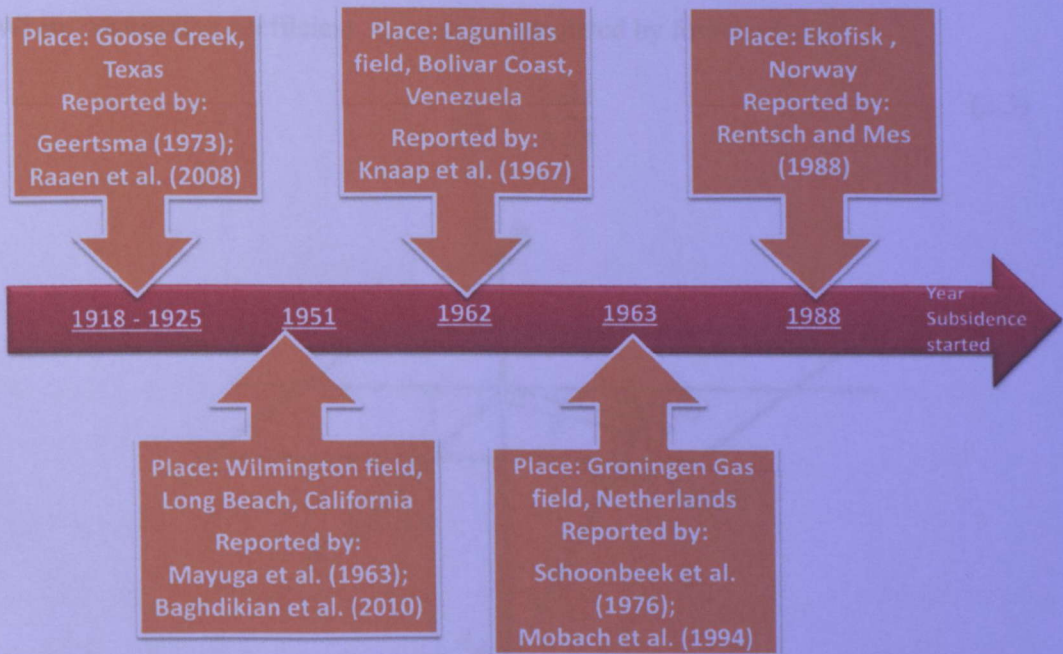


Figure 2.3 Places and time subsidence occurs in history

Most of the researches on subsidence are done solely or in partnership with multinational oil companies and most the data is confidential. Thus, it is not easy to obtain the field data.

2.3 Nucleus of Strain

In order to prevent or predict the subsidence occurrence, relationship between reservoir compaction and its subsidence is studied. Geertsma (1973) has used nucleus of strain (to calculate the both the vertical and horizontal displacement of the subsidence. According to Geerstma Nucleus of Strain (Geertsma, 1973; Reddish, 1994; Zoback, 2007), the vertical displacement, i.e. subsidence, due to a nucleus of strain of small but finite volume, d_v , under the influence of reservoir pressure reduction, ΔP , is

$$U_z(r, 0) = -\frac{1}{\pi} c_m (1 - \nu) \frac{D}{(r^2 + D^2)^{\frac{3}{2}}} \Delta p d_v \quad (2.1)$$

Similarly, displacement in horizontal direction can be calculated by

$$U_r(r, 0) = +\frac{1}{\pi} c_m (1 - \nu) \frac{D}{(r^2 + D^2)^{\frac{3}{2}}} \Delta p d_v \quad (2.2)$$

Where compaction coefficient, c_m , can be calculated by formula below

$$c_m = \frac{1}{z} \frac{dz}{dp} \quad (2.3)$$

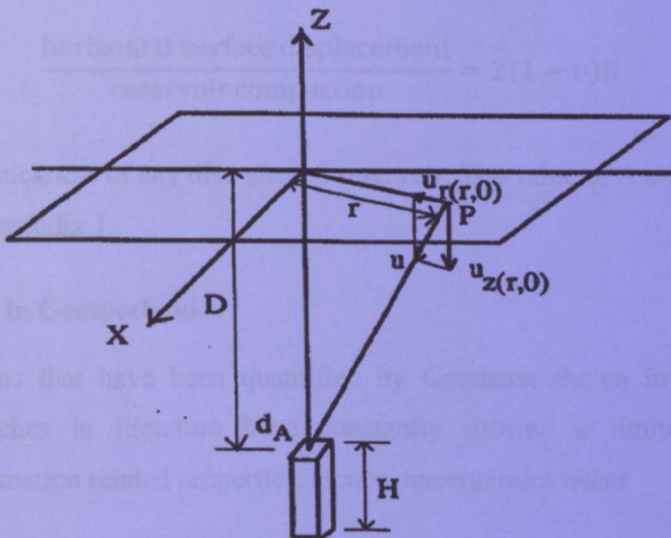


Figure 2.4 Geometry for Geertsma Solution by Geertsma (1973)

Where c_m is uniaxial compaction coefficient, which is dependent on factors like rock type, degree of cementation, porosity, and depth of burial. ν is Poisson's ratio of the reservoir rock; D is the depth of burial of the nucleus of strain, r is the radial distance from the vertical axis through the nucleus, Δp is the pore pressure reduction in the element, and d_v is the volume of the element.

2.3.1 Assumption of Geertsma Nucleus of Strain

There is one important assumption made in Geertsma model. Both the reservoir and its surroundings should be treated as homogeneous with regards to their deformation properties (Geertsma, 1973; Zoback, 2007, Raaen, 2008). Specifically, both c_m and ν should be treated as constant throughout the entire half-space.

By considering reservoir compaction to be $c_m \Delta p H$ (Geertsma, 1973, Reddish, 1994), an estimate between reservoir compaction and subsidence by can be amount to,

$$\frac{\text{vertical vertical displacement}}{\text{reservoir compaction}} = -2(1 - \nu)A \quad (2.4)$$

And similarly,

$$\frac{\text{horizontal surface displacement}}{\text{reservoir compaction}} = 2(1 - \nu)B \quad (2.5)$$

Where H is the thickness of any disc-shaped reservoir. The value of A and B is obtained using table in Appendix 1.

2.4 Uncertainty in Geomechanics

Despite equations that have been quantified by Geertsma shown in earlier section, previous researches in literature have constantly showed a limited data of the underground formation related properties. Hence, uncertainties occur.

It is know in industry that compaction coefficients is a function of porosity which in turn dependent on Young's Modulus. Such variability and complexity give rise to significant

variability and complex patterns of spatial correlation (Li and Tchelepi, 2003) due to heterogeneity of geological formation (Sarma et al., 2011). At the same time, Geomechanics model are far larger and extensive than the reservoir model. To perform accurate uncertainty analysis, a large number of simulations are often required. Thus, it is not economically feasible for Geomechanics models to run through the standard stochastic procedure to come to a probabilistic assessment. In oil and gas industry, the accuracy during the process of quantifying uncertainties is very important in making correct investment decisions. (Amudo et al., 2008).

2.5 Safety Factor and Probabilistic Geomechanics Methods

According to Kraft and Murff (1976), the conventional method for accounting for uncertainty is through the use of safety factor (F_s). Safety factor can be defined in many different ways. Generally, it is defined as (Narendranathan, 2009):

$$F_s = \frac{\text{Resisting Force}}{\text{Driving Force}} \quad (2.6)$$

However, research by D' Andrea and Sangrey (1974) pointed out that this measure is not always free of errors. It is supported by Ahilan (1993) that this approach of traditional deterministic safety factor does not take into consideration of variability occurred in strength and stress of the design, consequently underestimating the hidden risk. The traditional risk analysis uses only one single factor of safety in an analysis (Harrison and Wenner, 1996). Therefore, both variability and dependency of parameters should be included in estimating a real safety factor. The probabilistic approach constitutes an alternative to the traditional approach based on the safety factor. Rouaski and Belkacemi (2008) suggested that the principal difference between the probabilistic approach and the safety factor approach lies in the application of reliability theory, which allows uncertainties to be quantified consistently in a manner that is free from self-contradiction. They also made a comparison for different methods to examine their reliability index.

2.5.1 Design of Experiment (DOE) and Response Surface Method (RSM)

DOE is used together with RSM, which uses a statistical proxy equation to model the response as a function of uncertainties. DOE is a common method for studying subsurface uncertainties (Lawal, 2009). It is also an experimental design (Montgomery, 2001) used to efficiently collect experimental/simulation data to construct response surfaces with RSM, which is a collection of mathematical methods and statistical inferences (Friedmann and Li, 2005). Both DOE and RSM were initially and systematically presented by Box and Wilson (1951).

DOE has been used in petroleum industry since the early of 1990's in uncertainty analysis of performance forecasts of reservoirs, history matching, and well scheme optimization (Friedmann and Li 2005). Reservoir engineers have developed and successfully applied several experimental design workflows to various reservoir engineering studies. A typical workflow of DOE features the following steps:

1. Uncertainty framing
2. Screening parameters
3. Constraining uncertainty parameters
4. Risk analysis

Below is an example of DOE workflow by Itotoi et al. (2010) to manage reservoir uncertainty in gas field development. The first step is to identify potential key model parameters and their uncertainty ranges. It is followed by deciding type of design to use for creating the DOE table depending on the number of parameters. The table is then used to create a number of dynamic realizations resulting from the design. Simulations are then performed in the DOE table. After that, proxy (response equation) is generated for the objective function. It was done using LINEST function in Excel, essential regression and neural network. Monte-Carlo simulations are then performed on the proxy using the probability distribution of the parameters. Forecast from all dynamic realizations is then plotted.

Workflow for Experimental Design

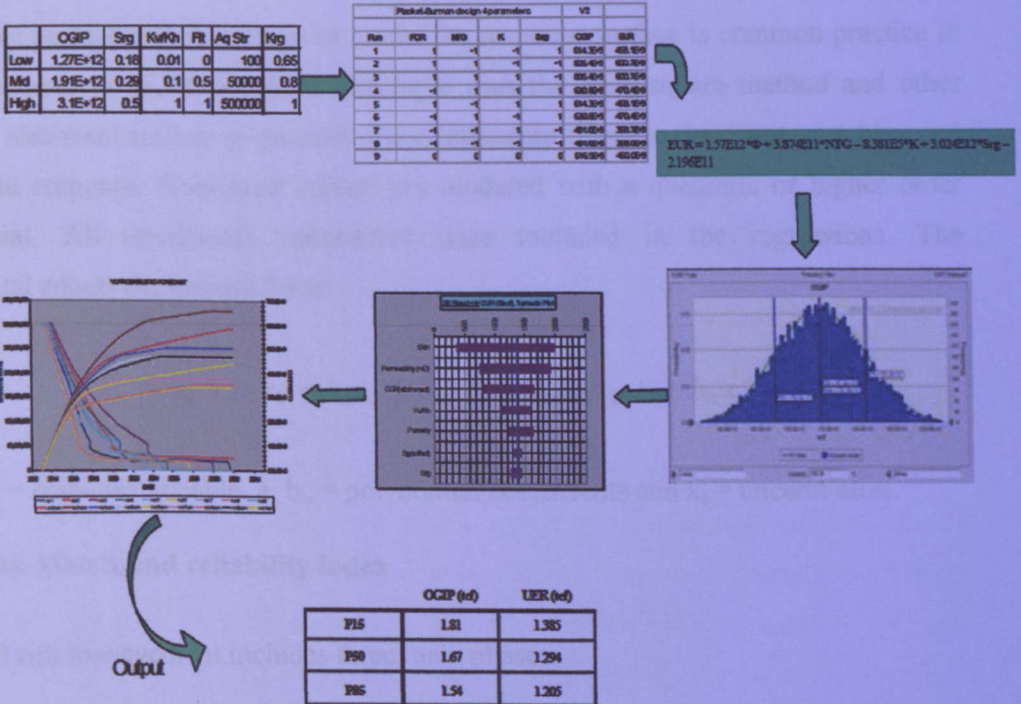


Figure 2.5 Example of DOE used in Gas Field Development by Itotoi et al. (2010)

The advantages of utilizing Design Of Experiment are:

1. Significantly reduces the number of simulations required to access uncertainties (Amudo, et al., 2008).
2. Able to extract maximum amount of unbiased information about the uncertainties from as few experiments as possible. (Amudo et al., 2008).
3. Systematically identify and rank the main input parameters that have the most impact on the reservoir performance
4. Generate a response surface model using the ranked parameters as independent variables to approximate the reservoir.

However the key disadvantage of this approach is that it does not take into consideration of the full probabilistic-density functions (PDFs) of the input random parameters.

2.5.2 Surface Response Model

The use of multi-linear regression to model the response surface is common practice in DOE (Carreras et al., 2006). This technique uses the least square method and other standard statistical testing to quantify the relationship between the input variables and the output response. Non-linear effects are modeled with a quadratic or higher order polynomial. All uncertainty parameters were included in the regressions. The polynomial adopts the general form:

$$y = b_0 + b_1x_1 + b_2x_2 + b_{11}x_1^2 + b_{12}x_1x_2 + \dots b_nx_n$$

Where y = response variable, a_i, b_i , = polynomial coefficients and x_i = uncertainties.

2.5.3 Risk Matrix and reliability index

Classical risk management includes three main phases:

- 1) A hazard assessment including a hazard analysis (Hazard characterization and frequency analysis) and a Consequence analysis (Consequence scenario and severity of consequences)
- 2) A risk assessment (risk estimation and tolerance criteria), and
- 3) A proper risk management plan through mitigation and feedback.

The most effective way to improve risk analysis is to improve the quality and quantity of the data, and to quantify the uncertainties (Cauquil, 2009).

Chapter 3: Methodology

3.1 Flow of Methodology

Preliminary research is first done to understand Geomechanics and problems associated with it. Method to solve the problems such as deterministic methods or probabilistic methods are then identified. After that, an identification of method to be used for de-risking flow should be done.

3.1.1 Geomechanics Model Building

A geomechanics model is build based on Geertsma Nucleus of Strain Model. The main focus of calculation in this report is Geertsma Displacement calculation. Once the model is built, the model is validated with several methods. The first one is through comparison of the results obtained from the textbook ‘Petroleum Related Rock Mechanics’ by Fjaer (2008). Next, field data is selected from previous journals to validate the model built.

3.1.2 Probabilistic Geomechanics Workflow

The workflow proposed in this project consists of five major components or steps, they are (A) Geomechanics Requirements; (B) Experimental Design; (C) Geomechanics Engine, (D) Multi-Variate Regression and (E) Reliability Assessment. Each of these components will be viewed as independent but separately relevant mechanism that will be integrated together for the reliability workflow. In Figure 3.1, an overview of the workflow is outlined. The function of each component will now be described.

Step A - Geomechanics Requirement

Due to inherent inhomogeneity and stochastic nature of geomaterials, geomechanics problems can be overwhelmingly complicated. First of all, the requirement for the geomechanics model need to be understood, and then we can gather the necessary data from field. The field data here is categorized into five major categories, (i) geologic

topology, (ii) in-situ stress measurements, (iii) formation properties, (iv) reservoir model(s) and (v) geomechanics laboratory measurements. The information is hard to be found complete from one literature due to the project confidentiality with companies. Extensive research and literature reviews are carried out in order to gather the relevant field data. Subsequent to the collection of field data, a base geomechanical model can then be built. The end product of Step A is thus a base geomechanical model. After the geomechanics model being built, we need to validate the model with the results obtained one from literature also. Thus, only after validation, we will proceed with next step.

Step B – Experimental Design

In the process of gathering information in Step A, especially when dealing with rock formation and unavailable of complete data, uncertainties occur. Design of Experiment will be utilized here to form a string of possible case scenarios. At this stage, it is important to decide what are the likely state variables that influence the experimental outcome. The end product of Step B is a design matrix.

Step C – Geomechanics Engine

Once the design matrix is available, numerical models with the appropriate variation in the parameters can be prototyped accordingly and executed in batch-mode using available geomechanics engine, e.g. GEOMECH and QuickBlock. The geomechanics engine will be treated as ‘black-box’ in this report. The output from Step C is the simulation results or the post-processed responses.

Step D - Multi-Variate Regression

From Step C, collections of post-processed responses are gathered. These responses can be subjected to the multi-variate regression analysis in Step D to produce (a) state variables sensitivity, (b) state variables relative influence, and (c) response surfaces. A proxy of specific response can be built based on the collective information in (a), (b) and

(c). A proxy is a linear approximation of specific observation in terms of the input state variables. It is the end product from Step D. In some situation, for very challenging geomechanical problem, it may be necessary to refine the proxy by going through Step B, C and D several times.

Step E - Reliability Assessment

Once the proxy from Step D is obtained, a limit state equation can to be defined accordingly. To proceed, the Probabilistic Density Function (PDF) of each state variable need to be supplied. For normal/lognormal PDF, the mean, μ_i , and standard deviation, σ_i , of the of state variable x_i are sufficient. For non-normal probabilistic distribution, additional statistical parameters must be supplied in order to define the PDF. In this report, a standard normal distribution is used because it has a very simple one-to-one transformation in the form

$$Z = \frac{x - \mu}{\sigma}$$

where Z is the transformed value in the standard normal curve with zero mean and unit standard deviation. With this information, the limit state equation can be solved either iteratively by numerical method or using Excel built-in solver.

Figure 3.1 illustrates the complete workflow that is proposed in this project.

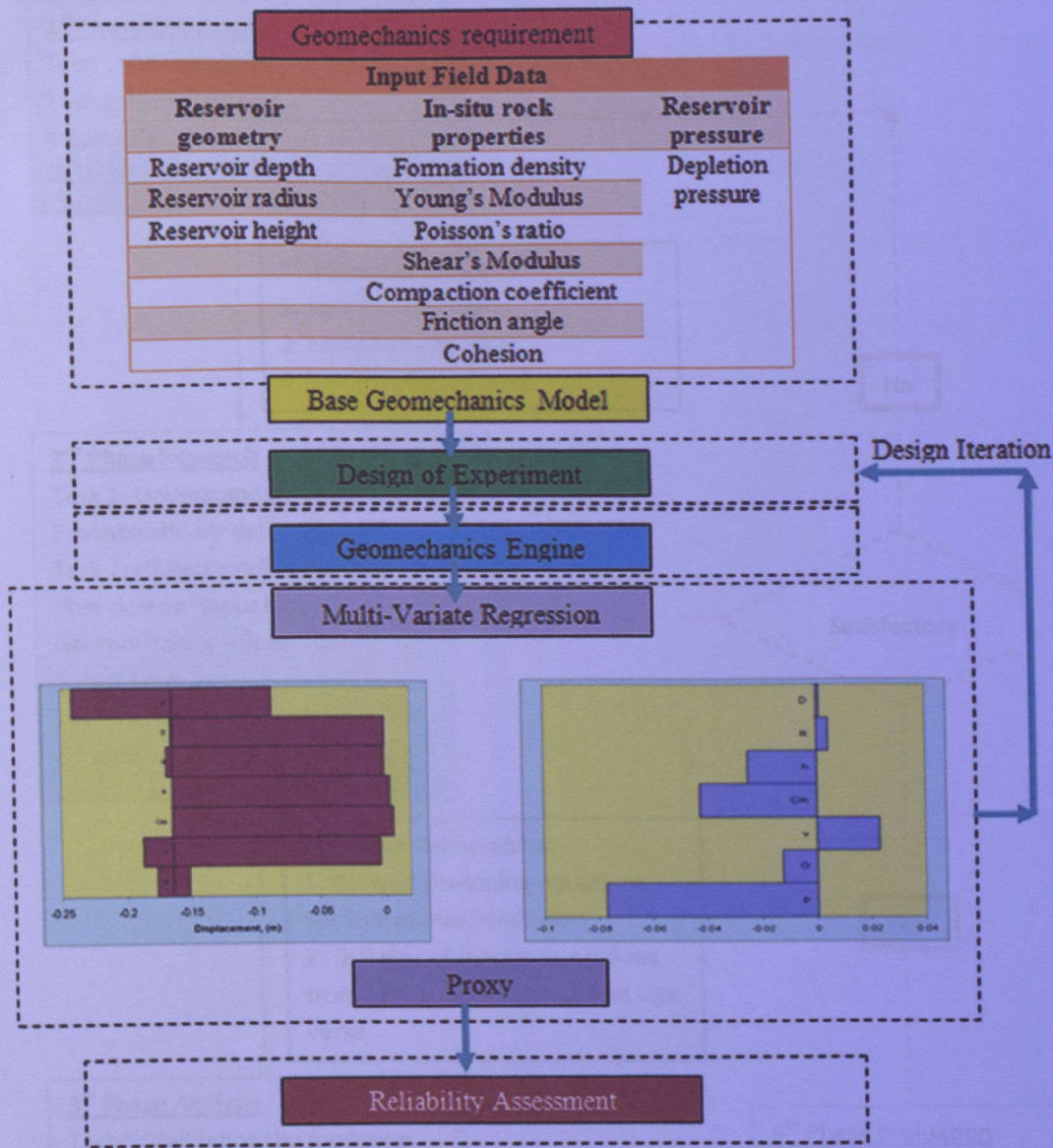


Figure 3.1 Proposed Geomechanics workflow

3.1 Preparing the Integrated Tools

Figure 3.2 is the flowchart of Methodology proposed for this project.

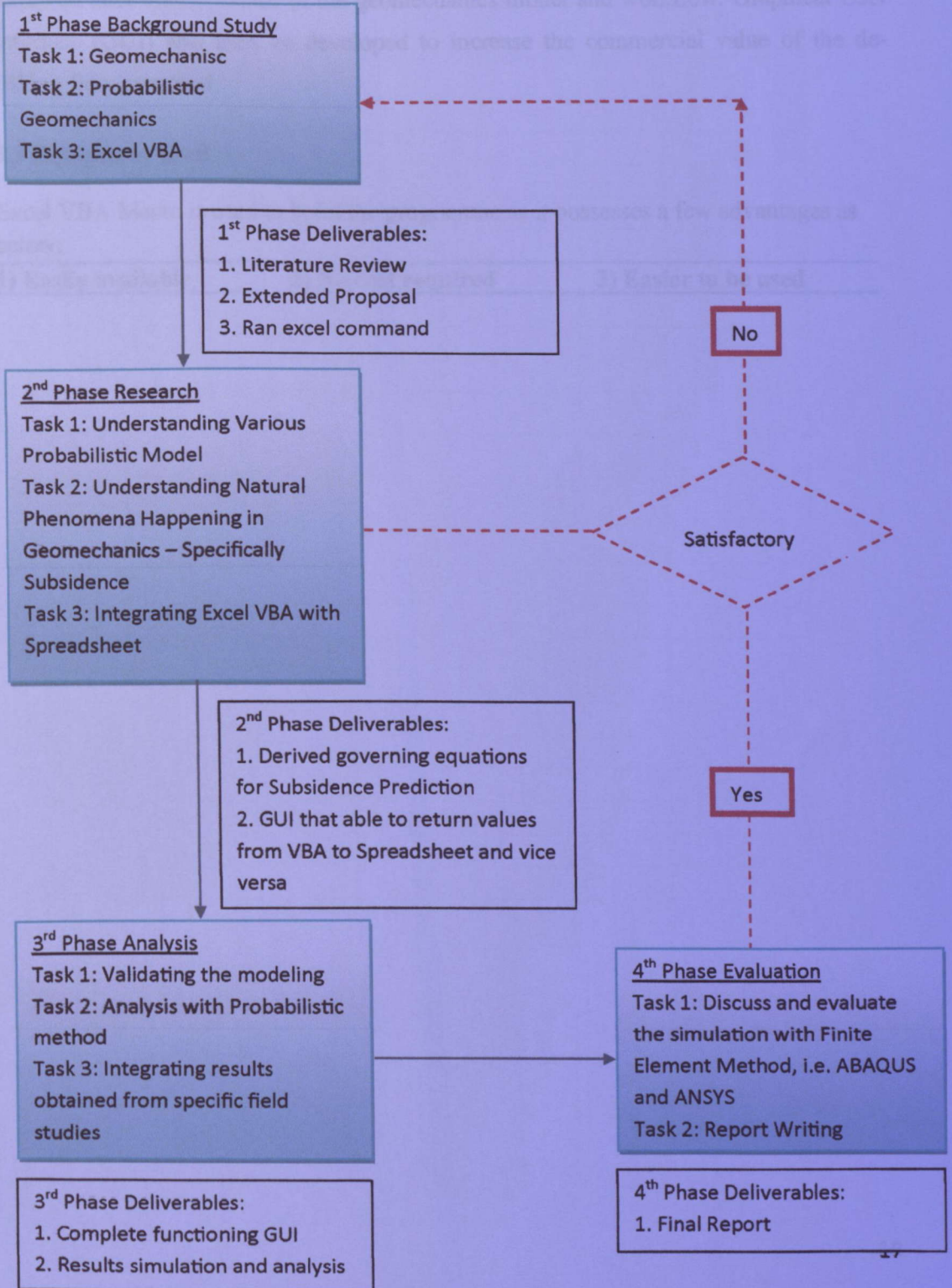


Figure 3.2 Methodology flow

3.2 Prototyping the Integrated Tools

Development of a prototype with Visual Basic for Application (VBA) should be followed after the definition of the geomechanics model and workflow. Graphical User Interface (GUI) will then be developed to increase the commercial value of the de-risking flow proposed.

3.3 Equipment Used

Excel VBA Macro is used to build the programme as it possesses a few advantages as below:

- | | | |
|----------------------------|----------------------------|-----------------------------|
| 1) Easily available | 2) No cost required | 3) Easier to be used |
|----------------------------|----------------------------|-----------------------------|

3.4 Gantt Chart



Chapter 4: Results and Discussion

4.1 Probabilistic Geomechanics Workflow

The geomechanical model first is built with good examples and validation. This model will then be defined with uncertainties occur throughout the formation. Uncertainties will be included in the input parameters. The Design of Experiment (DoE) is used to generate the design matrix with different combination of experiments for input parameters. This design matrix is then used to build the input table useful for the Geomechanics Engine execution. Then, the responses will be generated from this engine though the raw solutions inputted. Then, the completed design matrix continued with the MVR to generate the proxy function. Both upper and lower bound of the proxy are estimated through MVR. Then, it is followed by the FORM to compute the design points from the proxy. Simple Monte Carlo is simulated on the superimposed design points to form the design chart.

4.1.1 Geomechanics model

In Figure 4.1, the geomechanics model drawn is an axisymmetric model with a disk shape reservoir. The reservoir is buried at a depth D from the top surface, and extends at a radius R from its centre. The thickness of the reservoir is h . The base case of the geomechanical model is taken from Fjaer (2008), which is depicted in TABLE 1.

TABLE 1 Reservoir Properties for Analytical Solution from Fjaer (2008)

Reservoir Properties	Symbol	Unit	Values
Reservoir depth	D	m	2000
Reservoir radius	R	m	2000
Shear modulus	G	GPa	2
Poisson's Ratio	ν	-	0.25
Reservoir height	h	m	100
Depletion	ΔP	MPa	10
Density	ρ	kg/m ³	2200
Estimated compaction	$C_m h \Delta P$	m	0.17

Parameter	Low	High	Distribution	μ	σ
Reservoir Thickness (m)	50	120	Normal	100	15.625
Reservoir Depth (m)	1.8	2.2	Normal	2.0	0.1561
Reservoir Radius (m)	1.8	2.2	Normal	2.0	0.1561
Steel A-Modulus (GPa)	2.0	2.0	Normal	2.0	0.1961
Poisson Ratio	0.25	0.25	Normal	0.25	0.0391
Depletion Pressure (MPa)	10	10	Normal	10	0.5013
Uniaxial Compressive Strength (10^3 TPa)	1.2	2.2	Normal	1.7	0.39013

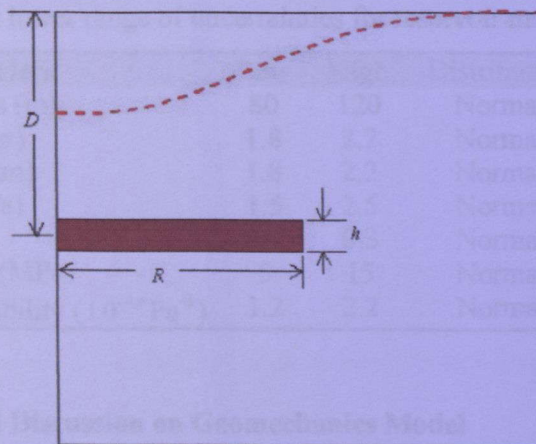


Figure 4.1 Geomechanical model for probabilistic analysis

The dotted line in Figure is the expected surface subsidence profile due to pressure depletion. For simplicity sake, the maximum surface subsidence, which located at the top-centre of the model is investigated. The surface subsidence of this model is given by Geertsma's analytical solution,

$$U_z = \frac{C_m R}{2} [-\epsilon I_3^{-\epsilon(z-c)} - (3 - 4\nu) I_3^{(z+c)} - 2z I_4^{(z+c)}] H \Delta P \quad (4.1)$$

Where I_3 and I_4 are the complex function of elliptic integrals.

In VBA calculation for this geomechanics model,

Young's Modulus is given by,

$$E = \frac{1}{C_m} \times \left[\frac{(1+\nu) \times (1-2\nu)}{1-\nu} \right] \quad (4.2)$$

And shear modulus is given by,

$$G = \frac{E}{2(1+\nu)} \quad (4.3)$$

In the geomechanics model for subsidence calculation, 7 uncertainties are, as shown in TABLE 2. The low and high values of the uncertainties are assumed P_{10} and P_{90} of a normally distributed curve, and the corresponding mean and standard deviation is found accordingly.

TABLE 2: Upper and lower range of uncertainties for reservoir model

Parameters	Low	High	Distribution	μ	σ
Reservoir Thickness (m)	80	120	Normal	100	15.625
Reservoir Depth (km)	1.8	2.2	Normal	2.0	0.1561
Reservoir Radius (km)	1.8	2.2	Normal	2.0	0.1561
Shear Modulus (GPa)	1.5	2.5	Normal	2.0	0.1951
Poisson Ratio	0.2	0.3	Normal	0.25	0.0391
Depletion Pressure (MPa)	5	15	Normal	10	3.9015
Uniaxial Compressibility (10^{-10} Pa^{-1})	1.2	2.2	Normal	1.7	0.39015

4.1.2 Validation and Discussion on Geomechanics Model

We will first test the accuracy of the VBA calculation with the analytical solution suggested by FJaer (2008) for subsidence calculation without taking into consideration of the uncertainties first. Four depletion pressure, ΔP are selected for this purpose. The depletion pressures are set at 10MPa, 20MPa, 30MPa, and 40MPa. The VBA calculation is tested by varying the depth of the reservoir. The results are shown in Figure 4.2. From Figure 4.2, both VBA calculation and analytical solution coincide each other at all the points. This shows that both of the calculations give the similar results.

To further depict the accuracy of the calculation, a graph of percentage deviation is plotted in Figure 4.3. It is shown that as the depth of the reservoir increases, the percentage of deviation increases.

However, the percentage difference is at most 0.1%. Thus, VBA calculation developed in Excel is reliable to be used to calculate the field subsidence.

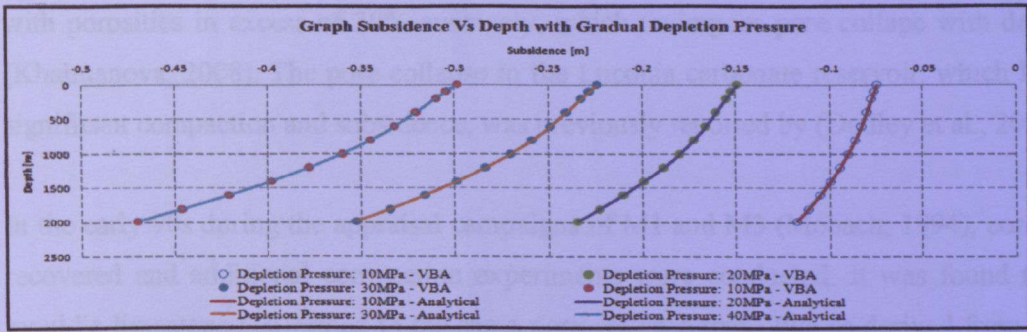


Fig. 4.2 Comparison of VBA calculation and Analytical Solution from FJaer (2008)

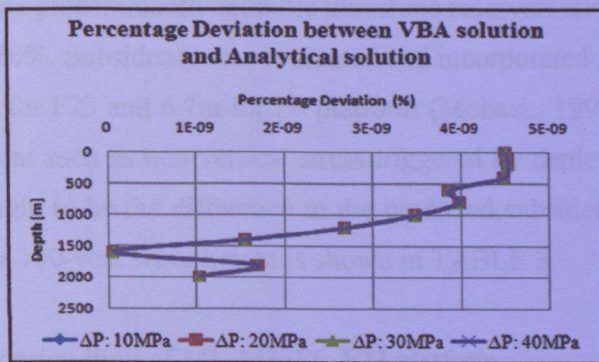


Fig. 4.3 Percentage deviation between VBA solutions and Analytical solutions

The results will compare the VBA model with previous research from Davidson et al. (2010), Dudley et al. (2009), Khalmanova (2008) and Mobach (1994) carried out in Gas Carbonate field located at Offshore Sarawak. Among the platform that will be examined are M1, M3, F6 and F23. We will first describe each platform briefly. Reservoir properties and rock mechanic properties of each platform will be described briefly too. All the properties discussed are based on the combination data obtained from (2010), Dudley et al. (2009), Khalmanova (2008) and Mobach (1994). All M1, M3, F6, F23 (Dudley et al., 2009) are located at the gas rich Central Luconia Province offshore Sarawak.

The fields are primarily of plat-form type buildup with single long gas column at depth of 1220-1830m (4000-6000 ft) overlying the aquifer. The Luconia carbonate has several facies, but its compaction properties are dominated by the mouldic limestone facies,

with porosities in excess of 30% averagely, which undergoes pore collapse with depletion (Khalmanova, 2008). The pore collapse in the Luconia carbonate reservoir, which leads to significant compaction and subsidence, was previously reported by (Dudley et al., 2009).

F23 has been producing since 1987 and has undergone a pressure depletion of about 9.3MPa (1350 psi). In the early 90s during the appraisal campaigns of M1 and M3 (Mobach, 1994), cores were recovered and additional compaction experiments were conducted. It was found that the mouldic limestone conformed to the same pore-collapse trend-like as derived from F6 and F23. Subsidence allowances were catered for the platform design of M1 at 5.8m and M3 of 2.6m. F6 and F23 are predominantly mouldic limestone reservoir with bulk-volume porosity in the range of 25-40%. Subsidence was evaluated and incorporated into the airgap design of the platform, 4.6m for F23 and 6.7m for F6 platform (Mobach, 1994). The model does not include other element such as non-vertical stress triggered by depletion and water invasion effect. This is thought to be the difference in the predicted subsidence. The air gap design limit in terms of the 100-year wave height is shown in TABLE 3.

TABLE 3 Air gap design limit of M1, M3, F6, F23 platform

	M1	M3	F6	F23
Design Limit	5.8m	2.6m	6.7m	4.6m

M1 is a carbonate reservoir at the top of a single large carbonate build-up at Offshore Sarawak, Malaysia (Mobach, 1994). Production started in 1996 in M1 field. Reservoir depth directly below the platform is around 1643m (4800 ft). The material parameters are estimated from well logs and laboratory core measurements. A porosity of 0.30 is used; friction angle and cohesion are based on values derived from the conventional tri-axial compression test data. Initial values for the Young's modulus, Poisson's ratio, are derived from the fit to core compaction test on the M1 well.

M3 has been producing since 1995 and has undergone pressure depletion of about 9.3MPa (1350 psi). At the end of year in 2004, the pressure is stabilizing at around 2460 psi. Nevertheless, GPS data show that subsidence continues to take place, suggesting a lag time

is required for reservoir compaction to translate to subsidence at surface. Ultimate subsidence is expected to stabilize around 3.35m (11ft).

F23 has been producing since 1983 and has undergone a pressure depletion of about 9.3MPa (1435 psi). This platform has the remaining production life of 2 years. The abandonment pressure was estimated to be at 2.07MPa (300psi), which is 14.8MPa (2150 psi) pressure depletion. If that is the case, the ultimate subsidence will exceed the design limit by 2-3 feet. A plot of failure data estimated the Mohr-coulomb shear failure that characterizes the friction angle and apparent cohesion (Dudley et al., 2009). Friction angle is estimated at 27 degrees with a safety factor of 4 degrees while cohesion is estimated at 14.8MPa (350psi) with a safety factor of 0.55MPa (80 psi) (Davidson et al., 2010). Mechanical properties of the overburden F23 platform are derived from the F23 overburden log data (Davidson et al., 2010) and underburden properties from the adjacent field data. Young's modulus varies from 0.86MPa to 8618MPa (125 to 1250 Kpsi) and Poisson's ratio varies from 0.31 to 0.42. A modified Cam-clay constitutive-model implementation is used for the Luconia Carbonate. Rock mechanic for F23 properties are shown in TABLE 4.

TABLE 4 Rock mechanic properties of F23

Reservoir Properties	Symbol	Unit	Carbonate Reservoir Model
Cohesion		psi	350
Friction Angle	-	Degrees	27
Poisson's Ratio	ν	-	0.21
Young's Modulus	E	Kpsi	499
Shear Modulus	G	Kpsi	227

F6 has been in production since 1987 (Davidson et al., 2010), and significant subsidence has been experienced already at 2.6m. F23 has an on-going monitoring program, including compaction logging data in the reservoir, GPS data on the platform, and sonar data for the platform height above sea level. The field monitoring program includes both reservoir compaction data from radioactive bullet logging, surface subsidence measurement from GPS, data and air gap measurement from sonar, and sonar survey data. Similar to F23, a modified Cam-clay constitutive model is used to describe the carbonate deformation behavior. The mechanic properties are shown in TABLE 5.

TABLE 5 Rock Mechanic properties of F6

Rock Mechanic Properties	Symbol	Unit	Carbonate Reservoir Model
Cohesion		psi	377
Friction Angle	-	Degrees	27
Poisson's Ratio	ν	-	0.21
Young's Modulus	E	Kpsi	550
Shear Modulus	G	Kpsi	227

Details of reservoir depletion pressure and its associated subsidence are tabulated in TABLE 6 and TABLE 7.

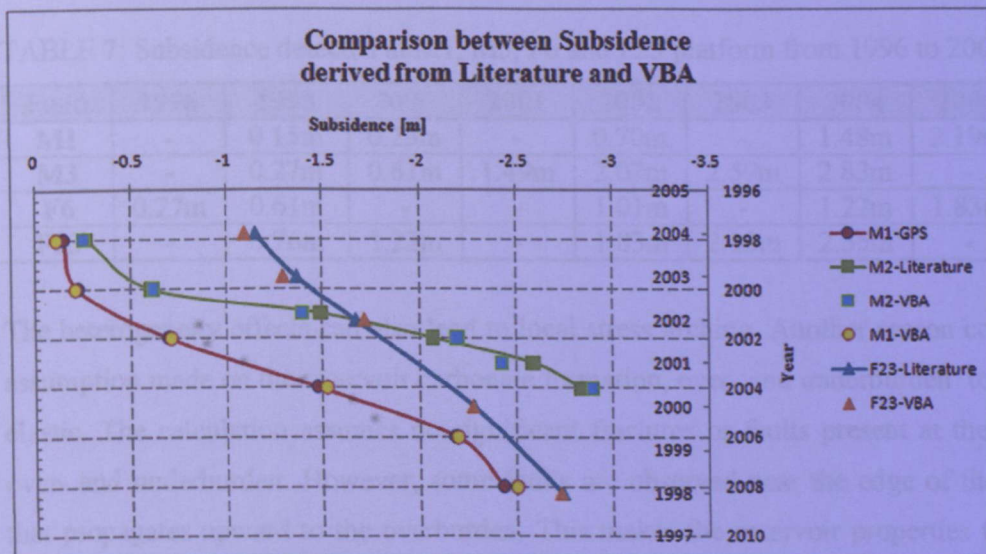


Fig. 4.4 Comparison between subsidences derived from GPS and VBA calculation

In figure 4.4, subsidence for F6 is not plotted as there are no data about its depletion pressure throughout the literature. From the graph plotted in figure 4.2, it clearly shows that the results obtained from VBA are consistent with the results obtained from literature review which were done through GPS monitoring method. The trend for both methods agrees that while the depletion pressure increases from year to year, the subsidence increases as well. When both results agree to each other, compressibility, porosity, Poisson's ratio, and also Young's modulus are observed to be changed from its initial value. Generally, compressibility increases and Young's modulus decreases.

In VBA method, for platform M1, the VBA calculation deviates gradually from the values obtained from literature review. To exhibit the sensitivity of the VBA calculation towards Young's Modulus and Poisson's Ratio, varying Poisson's ratio for M1 at 0.1, 0.15, 0.2, 0.25, 0.3, 0.35 and 0.4.

TABLE 6: Depletion pressure (in MPa) at M1, M3, F6 and F23 platform from 1996 to 2008

Field	1996	1998	2000	2001	2002	2003	2004	2006	2008
M1	-	-	-1.52	-	-2.59	-	-3.7	-4.10	-4.94
M3	-	-2.76	-6.90	-7.93	-8.62	-8.96	-9	-	-
F6	-	-	-	-	-	-	-	-	-
F23	-	-5.86	-7.58	-	-8.96	-9.45	-10.07	-	-

TABLE 7: Subsidence detected at M1, M3, F6 and F23 platform from 1996 to 2008

Field	1996	1998	2000	2001	2002	2003	2004	2006	2008
M1	-	0.15m	0.23m	-	0.70m	-	1.48m	2.19m	2.44m
M3	-	0.27m	0.61m	1.49m	2.07m	2.59m	2.83m	-	-
F6	0.27m	0.61m	-	-	1.01m	-	1.22m	1.83m	2.4m
F23	-	0.76m	1.22m	-	1.83m	2.13m	2.35m	-	-

The heterogeneity effects can also lead to local stress arching. Another reason could be the assumption made on the reservoir carbonate formation, over- and underburden to be linear-elastic. The calculation assumes no significant fractures or faults present at the reservoir, over- and underburden. However, some faults are observed near the edge of the reservoir that propagates upward to the overburden. This makes the reservoir properties to be more complicated and the results of subsidence to be inconsistent.

Initial measurements were available for the M3 and F23 platform. Although the GPS data gathered gave a good measurement and prediction for platform subsidence, the lack of initial data results a significant problem in comparing the initial subsidence of the platform.

Pore collapse would have occurred also at platform that have depleted for a long time with no pressure maintenance. Once pore collapse occurs, the compressibility can increase 10- to 100-fold. This greatly affects the evaluation of subsidence at the field.

4.3 DoE, Geomechanics Engine and MVR

Once the geomechanical model and its desirable observation are decided, the next step involves the generation of cases for experimentation. In this case, a Plackett-Burman design with 2 centre-points was used, resulting in 14 randomised cases, shown in Figure 4.5.

Case	ΔP (MPa)	D(km)	R (km)	H (m)	Poisson	Cm	G (GPa)	Surface Subsidence
1	5	1.8	2.2	120	0.20	2.2	1.50	-0.14433
2	15	2.2	2.2	120	0.20	1.2	1.50	-0.22341
3	10	2.0	2.0	100	0.25	1.7	2.00	-0.16484
4	5	2.2	2.2	80	0.20	1.2	2.50	-0.04965
5	10	2.0	2.0	100	0.25	1.7	2.00	-0.16484
6	5	1.8	1.8	80	0.20	1.2	1.50	-0.04965
7	15	1.8	1.8	80	0.20	2.2	2.50	-0.27306
8	15	2.2	1.8	120	0.20	1.2	1.50	-0.06516
9	15	1.8	2.2	120	0.20	2.2	1.50	-0.48841
10	15	2.2	1.8	120	0.30	1.2	2.00	-0.11329
11	5	1.8	1.8	120	0.30	2.2	1.50	-0.20665
12	5	2.2	1.8	80	0.20	2.2	2.00	-0.12359
13	15	1.8	2.2	80	0.20	1.2	2.00	-0.25258
14	5	2.2	2.2	80	0.30	2.2	2.50	-0.07964

Figure 4.5 Excel output of Plackett-Burman design

The geomechanical engine used for this exercise is the Excel-based Geertsma model, as shown in Figure .

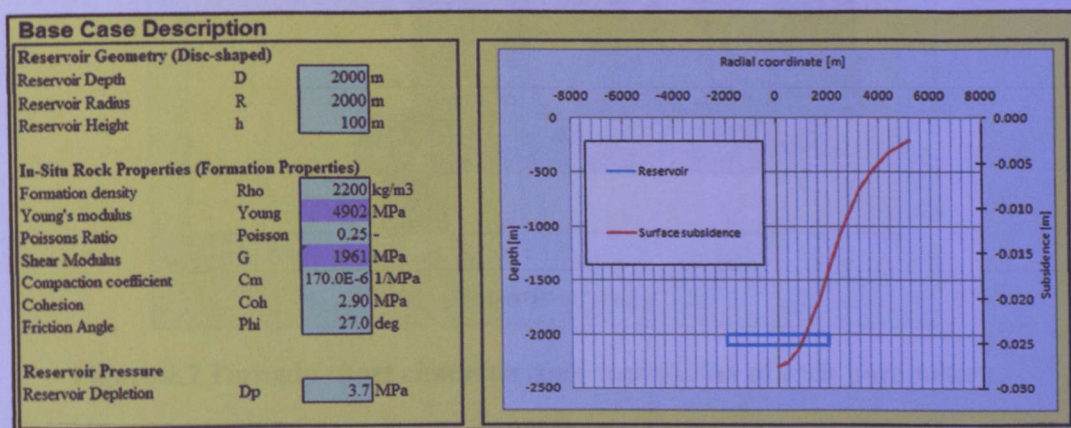


Figure 4.6 Excel based Geertsma geomechanical engine

The surface displacement obtained from the geomechanical engine can be found from the last column in Figure 4.5.

Once the solution is obtained, MVR can be carried out. This results in the following proxy for the subsidence in metre,

$$S = -0.016\Delta P + 0.005D + 0.023R - 0.001H + 0.479v - 0.088C_m - 0.026G \quad (4.4)$$

The graph of each regression is attached at Appendix back of this report.

From equation (4.4), a tornado chart and a parameters relative influence chart can be plotted as shown in Figure and Figure 4.8, respectively. The tornado chart characterizes the sensitivity of each factors with respect to the response. Notice that the mean-value of the response in Figure is approximately 0.15 m, which is given by the first term in the RHS of equation (4.4). The parameters relative influence chart is shown in Figure 4.8. It quantitatively characterizes the influence of each factors' uncertainty with respect to the response. A direct consequence of this is that the wider the spectrum of uncertainty, the higher is the relative influence.

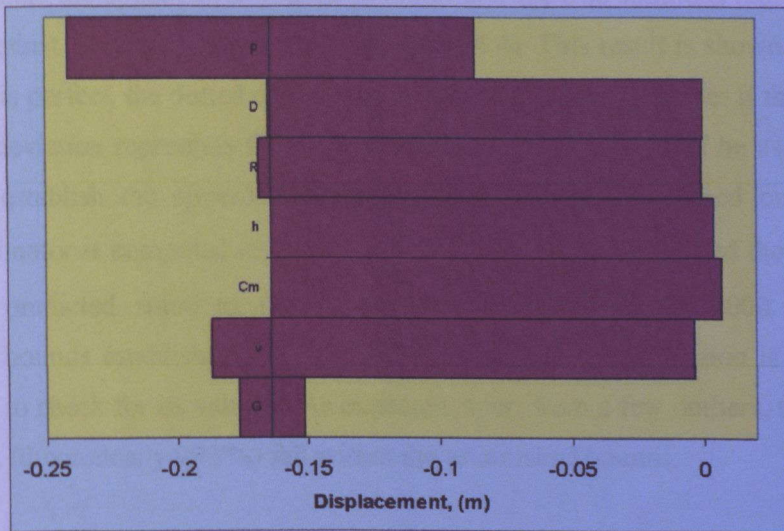


Figure 4.7 Tornado chart characterizing sensitivities of each parameters

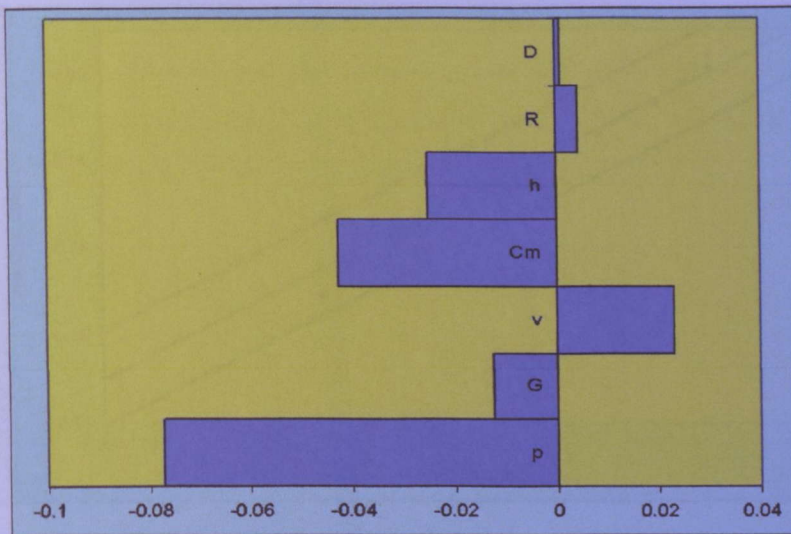


Figure 4.8 Relative influence chart characterizing the relative impact of each parameters

By careful study of Figure and Figure 4.8, it is not surprising to conclude that the state variable G may be a redundant parameter because in both chart, its sensitivity and relative influence are both minimal. This is verified by the analytical solution in equation 4.1. In order to estimate the upper/lower bounds to the proxy, the true solutions (equation 4.1) can be plotted against the predicted solutions (equation 4.4). This result is shown in Figure 4.9. If the match is perfect, the dotted data points will fall on the straight line. If the match is not perfect, the deviation represents the error of prediction. This error can be used as a priori-estimate to establish the upper/lower bounds of the prediction. Based on Figure , the unbiased estimator is computed to be $\sigma_E = 0.018103m$. Figure depicted the true solutions against the predicted solutions using Monte Carlo simulation of 8000 samples. The upper/lower bounds established from the experimental design simulation is superimposed onto Figure to check for its validity. As expected, apart from a few outliers, the majority of the solutions (theoretically 99.7%) fall within the established bounds.

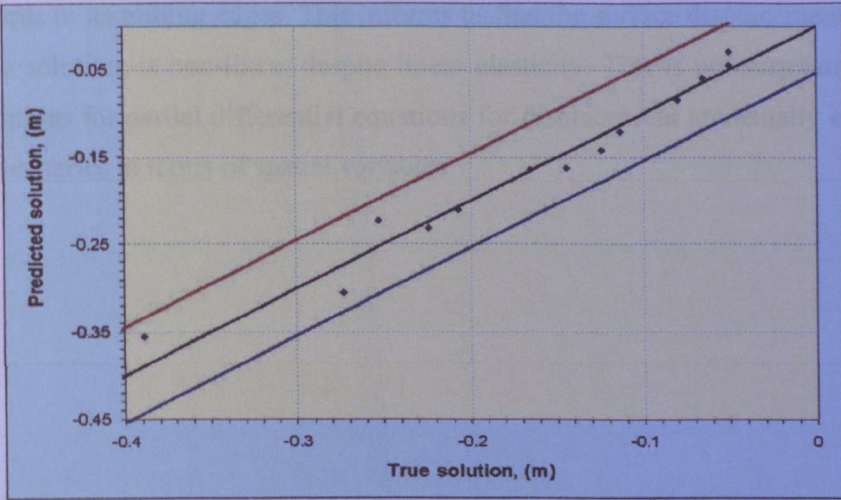


Figure 4.9 True solution against the predicted solution with upper/lower bounds

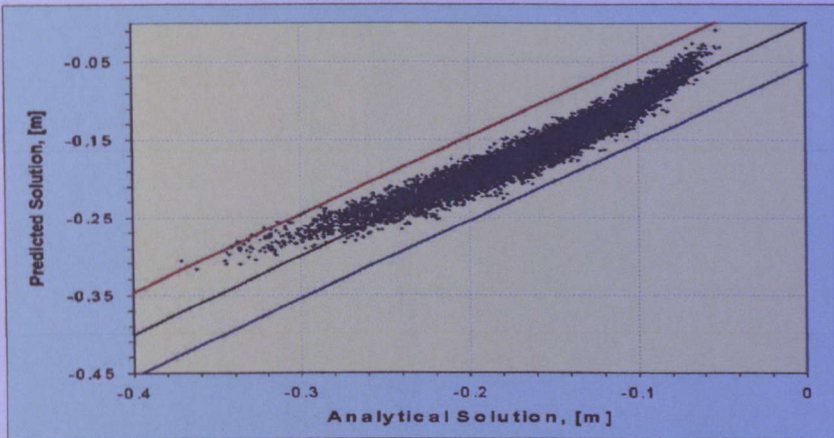


Figure 4.10 True solution against the predicted solution using Monte Carlo simulation. Upper/lower bounds established from experimental design simulation.

The unbiased estimator from Figure is calculated to be $\sigma_E^{MC} = 0.013556\text{m}$, which is smaller than σ_E . As the sample size increases, the error will approach a constant value. An additional point is that σ_E is a priori-estimate approaching the true error from above.

Figure 4.10 also reveals the nature of the surface displacement solution and its relation to the predicted solution. Even though the data points cluster around the line $y=x$, the cluster

bends upwards in its trailing edges. This informs us that the surface displacement, according to Geertsma solution, is non-linear despite linear elasticity. This is not surprising since the general solutions for partial differential equations for displacement are usually expressed in sum of power series in terms of spatial variables.

The whole project has the objective to include probabilistic face computing for geomechanics problems. Already discussed in the previous section are the calculation of the subsidence and incremental stress change. At this stage, the probabilistic software is still under development.

However, some preliminary UserForms has been generated using Excel VBA Programming. The User Form of the workflow is built and the first stage appearance is as below. This built for better user experience and ease of work.

The "Work Flow" icon is added into excel tab in order so that the users can use the system directly from Excel worksheet. The icon "PF" or its associated name "ProFlow" represents Probabilistic Workflow. "Linked Button Flow" will be replaced in the future to accommodate new work flow.



Figure 3.1 Excel Worksheet with Work Flow icon added

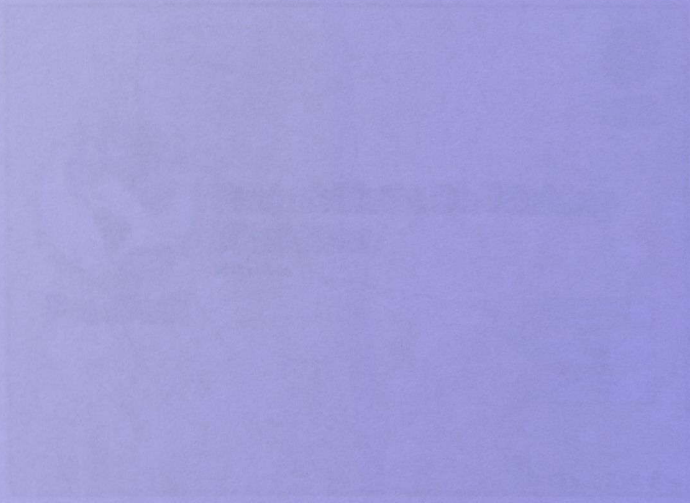


Figure 3.2 First stage of Work Flow

Chapter 5: Prototype

5.1 Probabilistic De-Risking Workflow, “ProWork”

The whole project has the objective to include probabilistic into de-risking for geomechanics problems. Already discussed in the previous section are the calculation of the subsidence and incremental stress change. At this stage, the probabilistic software is still under development.

However, some preliminary UserForm has been generated using Excel VBA Programming. The User Form of the workflow is built and the first stage appearance is as below. It is built for better user experience and ease of work.

The “Work Flow” add-in is added into excel tab in order so that the users can use the system directly from Excel worksheet. The Icon “Pw” or its associated name “ProFlow” represents Probabilistic Workflow. “Second Button Flow” will be replaced in the future to accommodate new work flow.

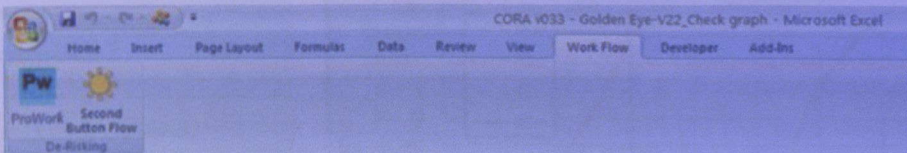


Figure 5.1 Excel Worksheet with Work Flow integrated

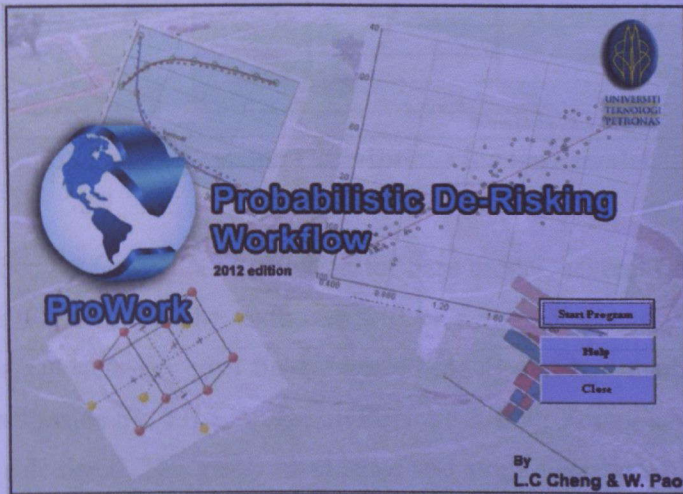


Figure 5.2 First Page of Work Flow

The first page is shown in Figure 5.2. with “Start”, “Help” and “Close” button.

5.2 Geomechanical Base Model

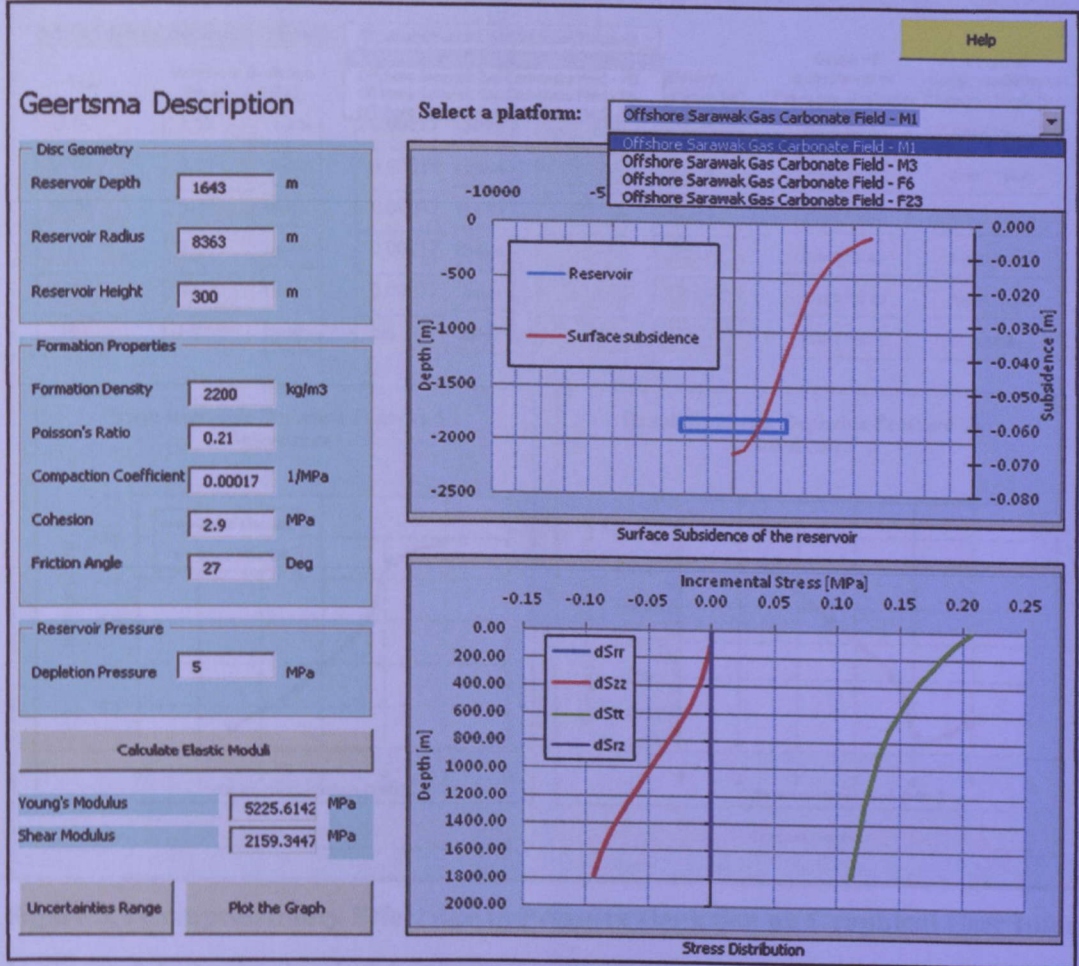


Figure 5.3 Geertsma Descriptions for base model

At the user interface for Geertsma Description for base model, several field data have been pre-input into the VBA so that the textboxes will be automatically populated with values once the choice is selected. For each field, Elastic Moduli will be calculated automatically through formula set inside the VBA. Shown in Figure 5.3, both Young's Modulus and Shear Modulus will be calculated. The graph subsidence and stress distribution are plotted on the right of the user interface.

Then, once the desired field data is selected, we can continue to examine the effect of pressure depletion on compressibility.

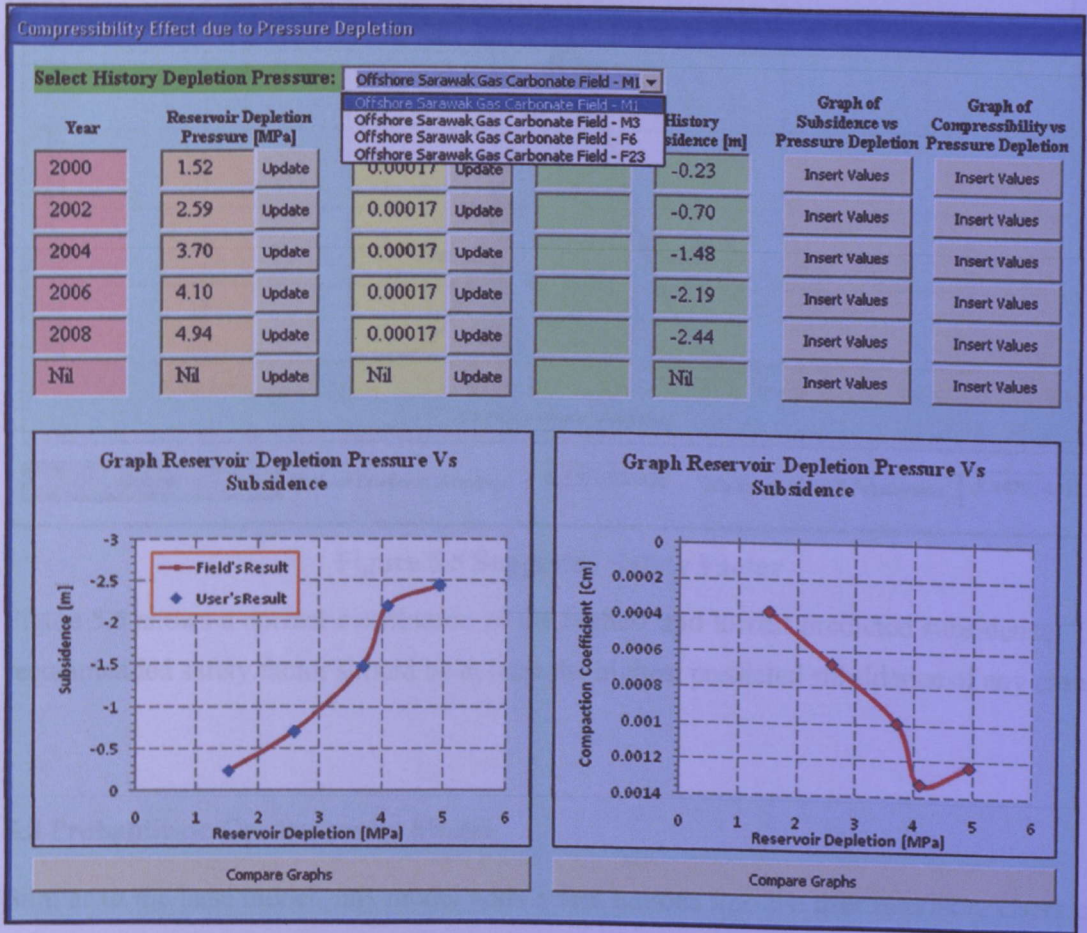


Figure 3.4 Compressibility Effect due to Pressure Depletion on Graphical User Interface

In Figure 5.4, the graphical user interface is auto-populated the history depletion pressure and its subsidence to the empty textboxes once the choice is chosen. The graph of the compressibility vs reservoir depletion is plotted. At the same time, graph of the predicted subsidence vs reservoir depletion with the Model built is also plotted.

For this user interface, a command button to recommend the safety factor for the platform to be built (based on the predicted subsidence) can be plotted also. The result is preliminary as it does not include the uncertainties that might be encountered. The uncertainties is discussed in the workflow in Chapter 4.

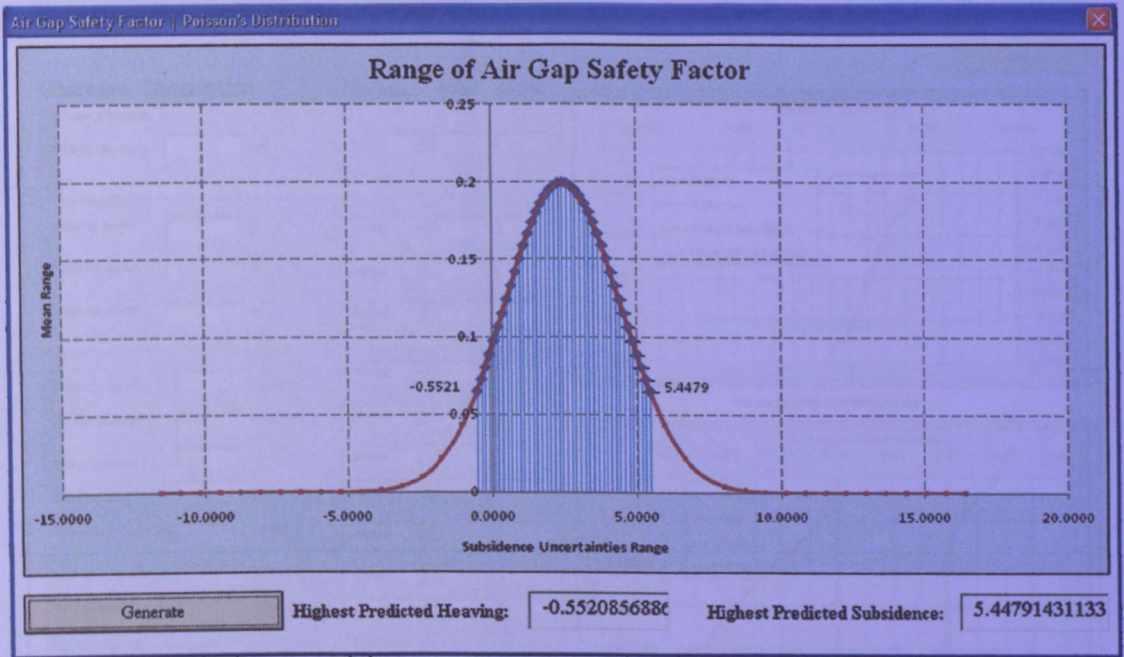


Figure 5.5 Suggested Safety Factor

Figure 5.5 shows a normal distribution of the highest and lowest predicted subsidence. The recommended safety factor should be at least the highest predicted subsidence of any case.

5.3 Probabilistic Geomechanics Model

Similar to the base model, this model adds a few buttons into the user interface. Users can enter the workflow by clicking “Start” Button straight away from the front page. When users clicked on the button, they will be prompted to the User Interface where users can key in the values to start analyzing the data. A graph will be plotted on the right of the User Interface. The graph is plotted on the right of the User Interface.

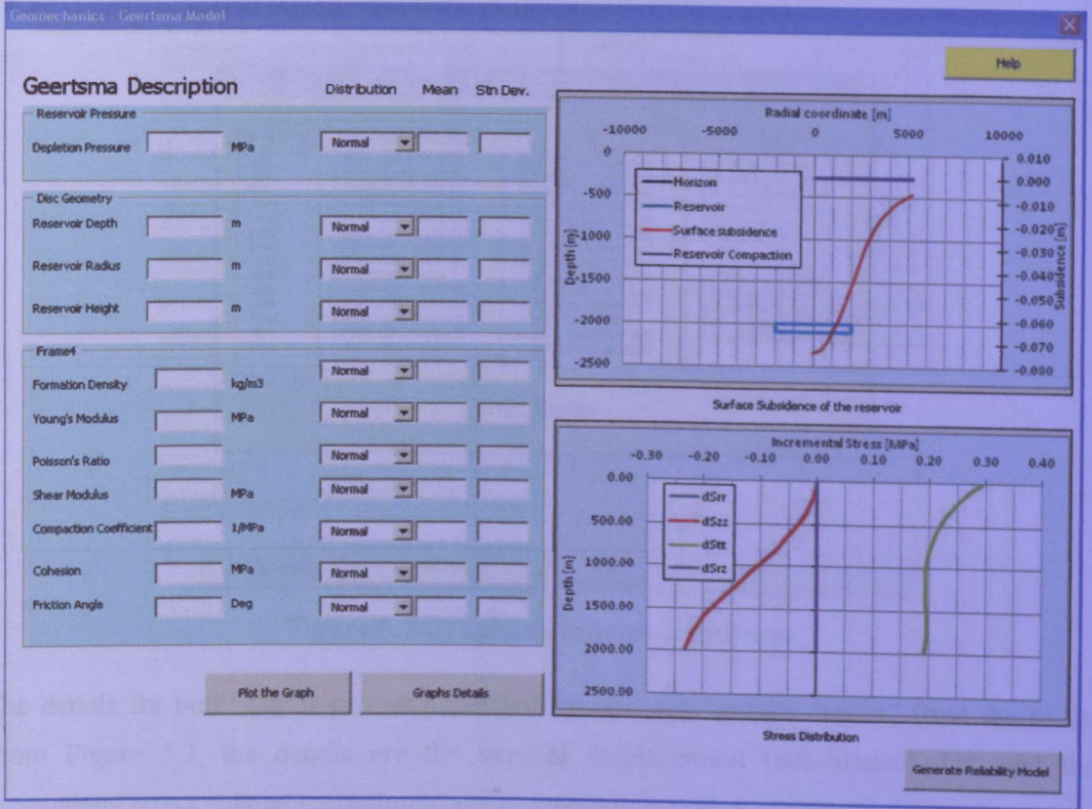


Figure 5.6 User Interface of De-Risking Workflow

The input data on the left column is the same for the input data available on figure 5.6. Distributions, mean and standard deviation are added into the UserForm as the previous results discussed is just part of the entire workflow proposed in methodology. Lognormal distribution will be used to determine the P10 and P90 of each property listed here.

On left columns are the graphs of subsidence and incremental stress just discussed in the section above. The graphs will be updated automatically everytime user press the “plot the graph” button. Each input box of the property is guided by a default value whenever user roll over the mouse at the empty input box.

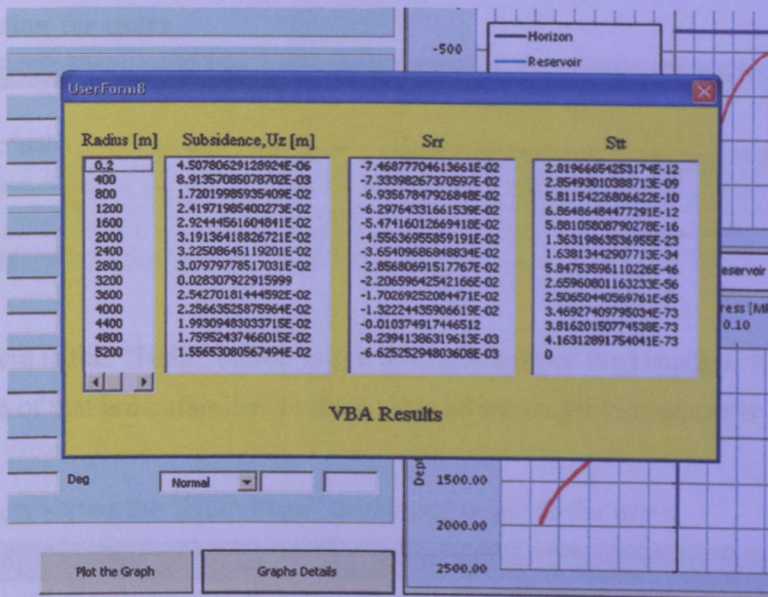


Figure 5.7 Graphs details on UserForm

The details for both graphs can be generated by clicking “graphs details” from the users. From Figure 5.7, the details are the vertical displacement (subsidence), Uz, and the incremental stress change according to varying reservoir radius.

After data input, calculation will be processed by VBA and general a complete reliability model with P10, P90, mean and standard deviation.

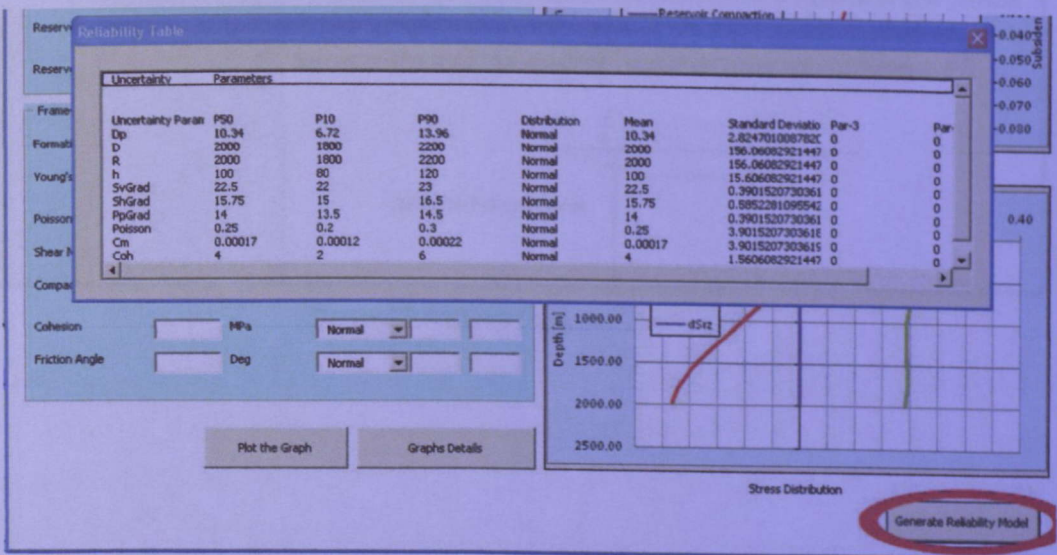
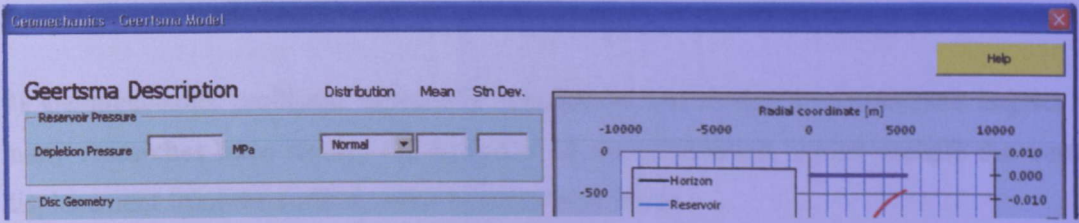


Figure 5.8 Reliability Table Generation

5.4 Help function for users



Notice that there is this “Help” button at the top right side of the program. It is to guide the users on topics of that are unfamiliar to them. One of the major topics here is subsidence.

Figure 5.9 below shows the “Help Page” developed to guide the users.

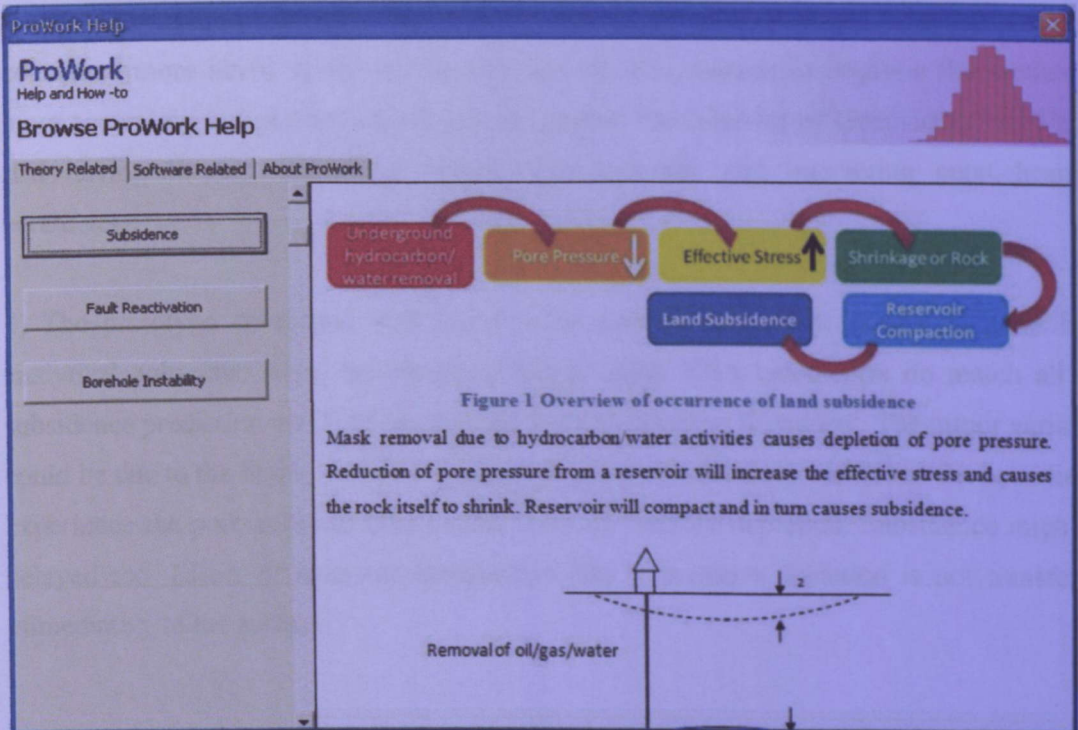


Figure 5.9 Help Page on ProWork

Chapter 6: Conclusion

1) Geomechanics problems especially subsidence has major environmental impact and many researches have studied the behavior of the subsidence, which include the vertical displacement from the surface and its related stress field.

2) In Geomechanics de-risking practice, this project has proposed an integrated tool of de-risking including reliability method, experimental design, multivariate regression, tornado chart, probabilistic density function (PDF), and First Order Reliability Method.

3) While the development of more sophisticated models also made by previous researchers concerned more about model uncertainty, we should continue to improve the method to more accurately and precisely represent and predict the behavior of Geomechanics. We are still having limited knowledge about many complex and interacting geomechanical parameters.

4) The prototype developed with Excel VBA portrays consistent results obtained from analytical solutions. Also, the results obtained using VBA calculation do match all the subsidence prediction and field monitoring done by previous literatures. The minor variation could be due to the highly complex geology in gas carbonate field which has the potential to experience the pore collapse after certain limit of pressure depletion. Subsidence might be delayed too. Effect of reservoir compaction due to pressure depletion is not transferred immediately to the surface.

6.1 Recommendation for Future Research

The solution nucleus of strain should be further studied to be able to generate the model of subsidence given an arbitrary point in the reservoir. Currently, the solution is based only on disk-shaped reservoir only so further research should also be carried out to any arbitrary shaped reservoir to approximate the real life example.

REFERENCES

- Aadnoy, B. (2011) Assessment and Mitigation of Drilling Risks Using ROP Model Coupled with Monte-Carlo Simulation. *ARMA*, 11-128.
- Ahilan, R. (1993) Development of Jackup Assessment Criteria Using Probabilistic Methods. *Offshore Technology Conference*, (7305), p.421-437.
- Amudo, C. et al. (2008) The Pains and Gains of Experimental Design and Response Surface Applications in Reservoir Simulation Studies. *SPE*, (118709).
- Arabnejad, H. (2010) Geotechnical Risks Analysis in Water Transfer Tunnel of The Kerman - Iran. *ISRM International*.
- Atashbari, V. et al. (2007) Subsidence Due To Fluid Withdrawal In Fractured Reservoirs. *SPE*.
- Baecher, G. (1982) Playing the Odds in Rock Mechanics. *Civil Engineering, Massachusetts Institute of Technology*, p.67-85.
- Baghdikian, S. et al. (2010) Enhancements to GPS-Based Subsidence Monitoring at the Wilmington Oil Field. *SPE*, (133131).
- Bell, F. et al. (2000) Mining subsidence and its effect on the environment: some differing examples. *Environmental Geology*, p.135-152.
- Bhattacharya, . and Singh, M. (1985) Development of Subsidence Damage Criteria. *Engineers International, Inc.*, (Contract J51120129)
- Box, G. and Wilson, K. (1951) On the Experimental Attainment of Optimum. *Royal Statistical Society*.
- Carreras, P. et al. (2006) Tahiti: Assessment of Uncertainty in a Deepwater Reservoir Using Design of Experiments. *SPE*, (102988).
- Cauquil, E. (2009) Risk Matrix for Non-Recurrent Geological Processes: Application to the Gas Hydrate Hazard. *Offshore Technology Conference*, (20014).
- D' Andrea, R. and Sangrey, D. (1974) Probabilistic Approach to the Undrained Bearing Capacity Problem. *ASCE*.
- Danielsen, J. et al. (1988) Reservoir Aspects Of Ekofisk Subsidence. *Offshore Technology Conference*.
- Davidson, J. et al. (2010) Ensuring Production in the Malaysia F6 field Using Field Monitoring and Geomechanical Forecasting. *SPE*, (132195).
- Derek, E. et al. (1989) Prediction Of Surface Movement With Emphasis On Horizontal Deformation Due To Mining. *American Rock Mechanics Association*.
- Dudley, J. et al. (2009) Predicting Accelerating Subsidence Above the Highly Compacting Luconia Carbonate Reservoirs, Offshore Sarawak Malaysia. *SPE Reservoir Evaluation and Engineering*.
- Einstein, H. (2003) Uncertainty in Rock Mechanics and Rock Engineering-Then and Now. *ISRM*, p.281-293.
- Fjaer, E. et al. (2008) *Petroleum Related Rock Mechanics*. 2nd ed. Amsterdam, The Netherlands: Elsevier.

- Friedmann, F. and Li, B. (2005) Novel Multiple Resolutions Design of Experiment? Response Surface Methodology for Uncertainty Analysis of Reservoir Simulation Forecasts. *SPE*, (92863).
- Geertsma, J. (1973) Land Subsidence Above Compacting Oil and Gas Reservoirs. *Petroleum Technology*, 3730 p.734-744.
- Goodman, H. et al. (2008) Deep Water Exploration Well Pre-Drill DST Sanding Potential Prediction using Monte Carlo Simulations. *ARMA*, (09-085).
- Harrison, J. and Wenner, D. (1996) Techniques to Cope with Uncertain Parameters in Geomechanics on Different Levels of Information. *ISBN*, (5410843 6), p.327-334.
- Helton, J. (2005) Sampling-Based Methods for Uncertainty and Sensitivity Analysis. *Sensitivity Analysis of Model Output*.
- Itotoi, I. et al. (2010) Managing Reservoir Uncertainty in Gas Field Development Using Experimental Design. *SPE*, (140619).
- Joseph, G. et al. (1972) An Approach to Analyzing Multiple Causes Of Subsidence. *SPE*.
- Khalmanova, D. and Dudley, J. (2008) Geomechanical modeling of subsidence and compaction in the M1 and Jintan gas fields, offshore Malaysia. *ARMA*, (08-192).
- Knaap, W. et al. (1967) On the Cause of Subsidence in Oil-Producing Areas.
- Kraft, L. and Murff, J. (1976) Probabilistic Investigation of Foundation Design for Offshore Gravity Structures. *SPE*, (5489), p.97-108.
- Lawal, K. (2009) Modelling Subsurface Uncertainties with Experimental Design: Some Arguments of Non-Conformists. (128350).
- Li, L. and Tchelep, H. (2003) Conditional Stochastic Moment Equations for Uncertainty Analysis of Flow in Heterogenous Reservoirs. *SPE*, (87337), p.392-400.
- Macary, S. et al. (1999) Better Understanding of Reservoir Statistics is the Key for Reliable Monte Carlo Simulation. *SPE*, (53264).
- McLellan, P. et al. (1998) Application of Probabilistic Techniques for Assessing Sand Production and Borehole. *SPE*, (47334), p.143-151.
- Mobach, E. and Gussinklo, H. (1994) In-situ Reservoir Compaction Monitoring in the Groningen Field. *SPE*, 28094 p.535-547.
- Montgomery, D. (2001) *Design and Analysis of Experiments*. 5th ed. John Wiley & Sons, INC..
- Narendranathan, S. (2009) Fundamentals of Probabilistic Slope Design & its Use in Pit Optimization. *ARMA*, (09-008).
- Raaen, A. et al. (2008) *Petroleum Related Rock Mechanics*. 2nd ed. Elsevier, p.391.
- Rouaski, L. and Belkacemi, S. (2008) Reliability Analysis of Rock Foundation. *ISRM International*, p.973-979.
- Reddish, D. et al. (1994) Computerized prediction of subsidence over oil and gas fields. *SPE*, 28105.
- Rentsch, H. and Mes, M. (1988) Measurement of Ekofisk Subsidence. *Offshore Technology Conference*, 5619 p.23-30.

Salteli, A. (2002) Sensitivity Analysis for Importance Assessment. *Risk Analysis*, 22 (3), p.579-590.

Sarma, P. et al. (2011) A Comparative Study of the Probabilistic-Collocation and Experimental-Design Methods for Petroleum-Reservoir Uncertainty Quantification. *SPE*, (140738), p.429-439.

Schoonbeek, J. (1976) Land Subsidence as a Result of Natural Gas Extraction in the Province of Groningen. *SPE of AIME*, 5751.

Shinkle, K. and Dokka, R. (2004) Rates of vertical displacement at benchmarks in the lower Mississippi Valley and the northern Gulf Coast.. *National Oceanic and Atmospheric Administration Tech*, Rept 50.

Wing, A. (2005) *Production-Induced Reservoir Compaction, Permeability Loss and Land Surface Subsidence*. Ph.D Dissertation. Stanford University.

Mah, K. and Draup, A. (2004) Managing Subsidence Risk in Gas Carbonate Fields Offshore Sarawak. *SPE*, (88573).

Zoback, M. (2012) *Reservoir Geomechanics*. Cambridge, England: Cambridge University Press.

TABLE 1. Comparison of the results of the different methods for the estimation of the uncertainty in the permeability field. The results are presented in terms of the mean and standard deviation of the permeability field. The results are presented in terms of the mean and standard deviation of the permeability field. The results are presented in terms of the mean and standard deviation of the permeability field.

Method	Mean	Std	2.3	1.9	1.5	1.2	1.0	0.8	0.6	0.5
MC	1.000	0.100	0.700	0.500	0.300	0.100	0.000	0.000	0.000	0.000
CE	1.000	0.100	0.700	0.500	0.300	0.100	0.000	0.000	0.000	0.000
ED	1.000	0.100	0.700	0.500	0.300	0.100	0.000	0.000	0.000	0.000
PC	1.000	0.100	0.700	0.500	0.300	0.100	0.000	0.000	0.000	0.000
CE-ED	1.000	0.100	0.700	0.500	0.300	0.100	0.000	0.000	0.000	0.000
CE-PC	1.000	0.100	0.700	0.500	0.300	0.100	0.000	0.000	0.000	0.000
ED-PC	1.000	0.100	0.700	0.500	0.300	0.100	0.000	0.000	0.000	0.000
CE-ED-PC	1.000	0.100	0.700	0.500	0.300	0.100	0.000	0.000	0.000	0.000

APPENDIX
APPENDIX I

Geertsma Nucleus of Strain Model

$$\frac{\text{vertical displacement}}{\text{reservoir compaction}} = -2(1 - \nu)A$$

$$\frac{\text{horizontal displacement}}{\text{reservoir compaction}} = 2(1 - \nu)B$$

TABLE 1—VALUES OF $A = R \int_0^{\infty} J_1(\alpha R) J_0(\alpha r) e^{-\rho \alpha} d\alpha$ FOR RANGES OF VALUES OF $\rho = r/R$ AND $\eta = D/R$

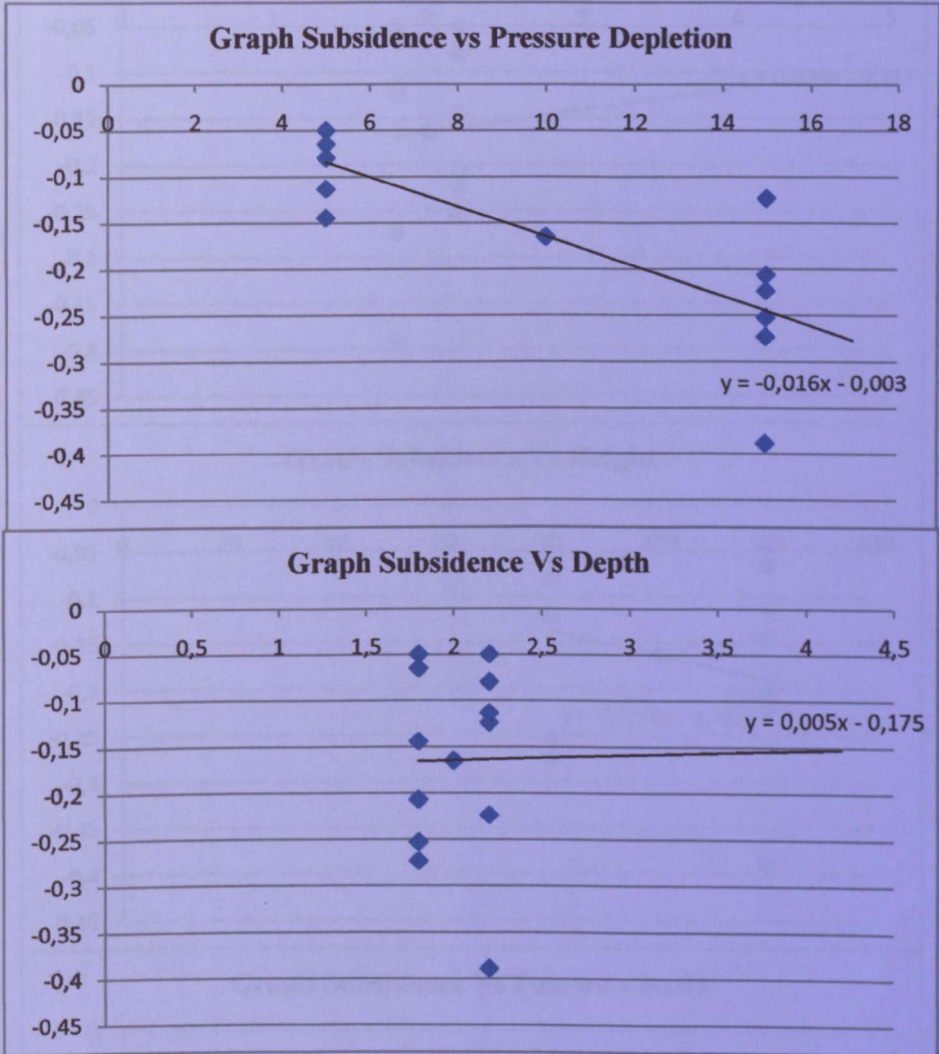
ρ	η											
	0.0	0.2	0.4	0.6	0.8	1.0	1.2	1.4	1.6	1.8	2.0	3.0
0.0	1.0000	0.8039	0.6286	0.4855	0.3753	0.2929	0.2318	0.1863	0.1520	0.1258	0.1056	0.0513
0.2	1.0000	0.7983	0.6201	0.4771	0.3683	0.2876	0.2279	0.1835	0.1500	0.1244	0.1045	0.0510
0.4	1.0000	0.7789	0.5924	0.4508	0.3473	0.2720	0.2167	0.1754	0.1442	0.1202	1.1014	0.0502
0.6	1.0000	0.7349	0.5377	0.4043	0.3124	0.2470	0.1989	0.1628	0.1351	0.1135	0.0965	0.0488
0.8	1.0000	0.6301	0.4433	0.3368	0.2658	0.2147	0.1762	0.1465	0.1234	0.1049	0.0901	0.0470
1.0	0.5000	0.3828	0.3105	0.2559	0.2130	0.1787	0.1510	0.1286	0.1102	0.0951	0.0827	0.0449
1.2	0.0000	0.1544	0.1871	0.1795	0.1621	0.1433	0.1257	0.1103	0.0965	0.0848	0.0748	0.0424
1.4	0.0000	0.0717	0.1101	0.1216	0.1197	0.1120	0.1024	0.0925	0.0831	0.0744	0.0667	0.0398
1.6	0.0000	0.0400	0.0682	0.0829	0.0876	0.0865	0.0824	0.0768	0.0707	0.0646	0.0589	0.0370
1.8	0.0000	0.0249	0.0449	0.0580	0.0647	0.0668	0.0659	0.0633	0.0597	0.0557	0.0516	0.0343
2.0	0.0000	0.0168	0.0312	0.0418	0.0485	0.0519	0.0528	0.0520	0.0502	0.0477	0.0450	0.0315
3.0	0.0000	0.0042	0.0082	0.0118	0.0149	0.0174	0.0193	0.0207	0.0216	0.0221	0.0222	0.0198

TABLE 2—VALUES OF $B = R \int_0^{\infty} J_1(\alpha R) J_1(\alpha r) e^{-\rho \alpha} d\alpha$ FOR RANGES OF VALUES OF $\rho = r/R$ AND $\eta = D/R$

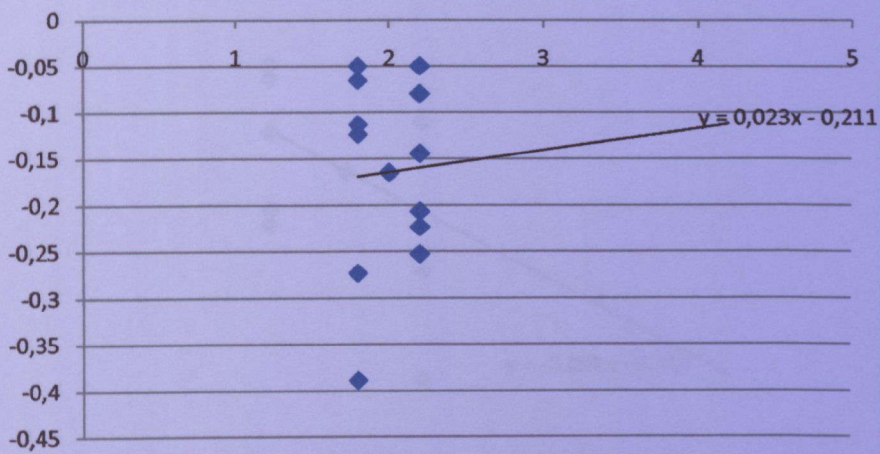
ρ	η											
	0.0	0.2	0.4	0.6	0.8	1.0	1.2	1.4	1.6	1.8	2.0	3.0
0.0	0.0000	0.0000	0.0000	0.0000	0.0000	0.0000	0.0000	0.0000	0.0000	0.0000	0.0000	0.0000
0.2	0.1015	0.0954	0.0804	0.0628	0.0472	0.0350	0.0259	0.0194	0.0147	0.0113	0.0089	0.0032
0.4	0.2134	0.1979	0.1622	0.1238	0.0917	0.0675	0.0500	0.0375	0.0285	0.0220	0.0173	0.0062
0.6	0.3530	0.3163	0.2443	0.1789	0.1298	0.0949	0.0703	0.0529	0.0405	0.0314	0.0248	0.0090
0.8	0.5721	0.4573	0.3151	0.2197	0.1570	0.1147	0.0854	0.0648	0.0500	0.0391	0.0311	0.0117
1.0	∞	0.5456	0.3422	0.2355	0.1693	0.1252	0.0945	0.0726	0.0567	0.0448	0.0359	0.0139
1.2	0.5235	0.4278	0.3072	0.2237	0.1666	0.1265	0.0976	0.0764	0.0605	0.0485	0.0393	0.0158
1.4	0.3293	0.3026	0.2482	0.1958	0.1535	0.1208	0.0958	0.0766	0.0619	0.0504	0.0414	0.0174
1.6	0.2338	0.2228	0.1962	0.1650	0.1358	0.1110	0.0907	0.0743	0.0611	0.0506	0.0422	0.0185
1.8	0.1767	0.1711	0.1566	0.1377	0.1180	0.0997	0.0838	0.0703	0.0590	0.0496	0.0420	0.0184
2.0	0.1390	0.1358	0.1272	0.1152	0.1018	0.0885	0.0762	0.0653	0.0559	0.0478	0.0410	0.0199
3.0	0.0580	0.0576	0.0562	0.0541	0.0514	0.0483	0.0449	0.0414	0.0380	0.0346	0.0314	0.0190

APPENDIX 2

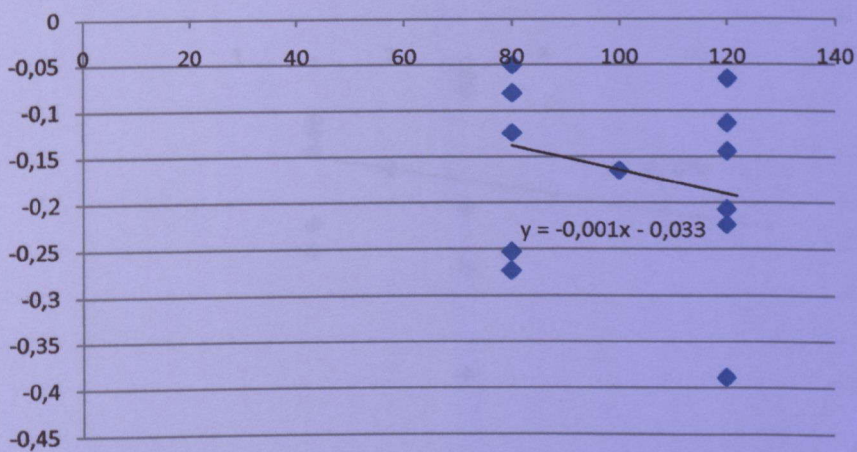
Multi-linear Regression to generate equation 4.4



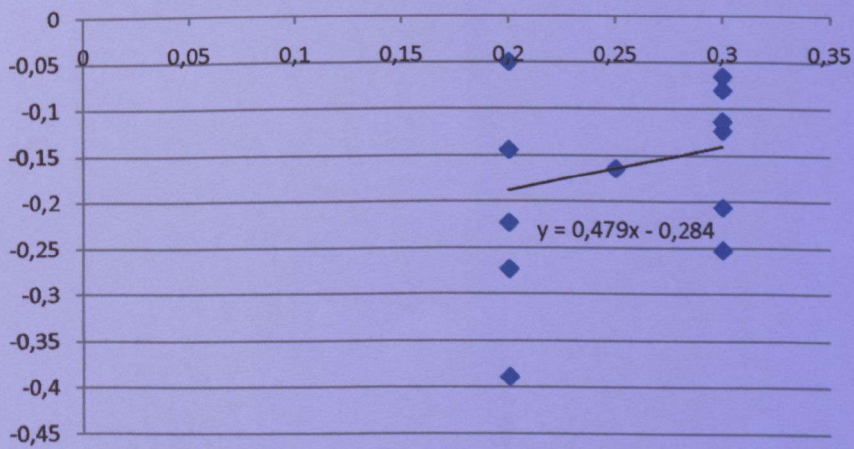
Graph Subsidence Vs Radius



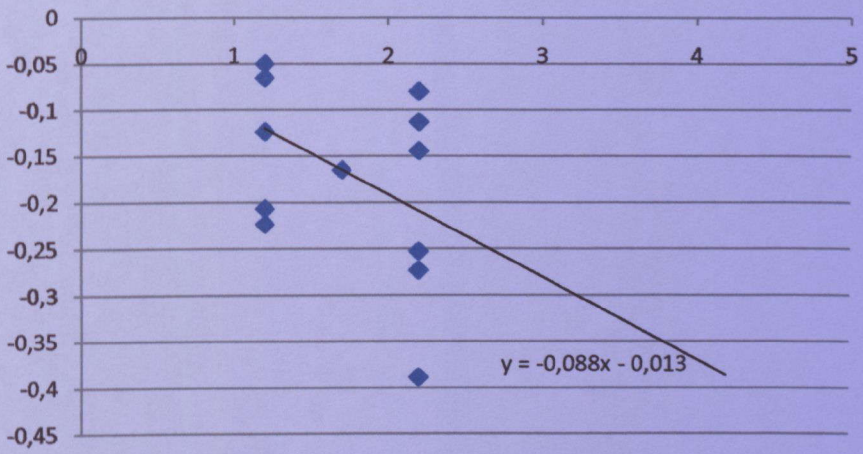
Graph Subsidence Vs Height



Graph Subsidence Vs Poisson's Ratio



Graph Subsidence Vs Compressibility



Graph Subsidence Vs Shear Modulus

